nature plants

ARTICLES

https://doi.org/10.1038/s41477-019-0546-1

Proteasome subunit RPT2a promotes PTGS through repressing RNA quality control in *Arabidopsis*

Myung-Hee Kim[1], Jieun Jeon[1,2], Seulbee Lee[1], Jae Ho Lee[1,2], Lei Gao[3], Byung-Hoon Lee[2], Jeong Mee Park[4], Yun Ju Kim[1*] and June M. Kwak[2*]

RNA quality control (RQC) and post-transcriptional gene silencing (PTGS) target and degrade aberrant endogenous RNAs and foreign RNAs, contributing to homeostasis of cellular RNAs. In plants, RQC and PTGS compete for foreign and selected endogenous RNAs; however, little is known about the mechanism interconnecting the two pathways. Using a reporter system designed for monitoring PTGS, we revealed that the 26S proteasome subunit RPT2a enhances transgene PTGS by promoting the accumulation of transgene-derived short interfering RNAs without affecting their biogenesis. RPT2a physically associated with a subset of RQC components and downregulated the protein level. Overexpression of the RQC components interfered with transgene silencing, and impairment of the RQC machinery reinforced transgene PTGS attenuated by *rpt2a*. Overall, we demonstrate that the 26S proteasome subunit RPT2a promotes PTGS by repressing the RQC machinery to control foreign RNAs.

Post-transcriptional gene silencing (PTGS) is a regulatory mechanism that suppresses invasive RNAs, including transgene-derived and viral RNAs, and also controls endogenous RNAs involved in stress responses and development. PTGS acts through short interfering RNAs (siRNAs) and microRNAs (miRNAs). In plants, the prerequisite step for initiating siRNA-mediated PTGS is the conversion of single-stranded RNAs to double-stranded RNA, which is accomplished by SUPPRESSOR OF GENE SILENCING 3 (SGS3) and RNA DEPENDENT RNA POLYMERASE 6 (RDR6). In turn, DICER-LIKE 2 (DCL2) or DCL4 processes the double-stranded RNAs to 21–22 nucleotide (nt) siRNAs, which are eventually incorporated into ARGONAUTE 1 (AGO1) for facilitating the cleavage of target RNAs[1]. The initial silencing signal spreads to nearby cells and then is amplified through the production of secondary siRNAs, further enforcing systemic RNA silencing[2]. This amplification process (also known as transitivity) is critical for the enhancement of PTGS triggered by sense transgenes (S-PTGS) and for antiviral defence.

RNA quality control (RQC) is an evolutionarily conserved RNA surveillance mechanism that detects and removes endogenous aberrant RNAs to prevent the production of potentially toxic proteins[3]. The major structural features of functional messenger RNAs include the 5′ cap and 3′ poly(A) tail, which contribute to mRNA integrity and facilitate translation. Aberrant RNAs defective in either or both these structures are recognized by the RNA decay machinery and degraded by conserved exo-ribonucleases. In plants, the removal of the 5′ cap structure and 3′ poly(A) tail is accomplished by conserved components of the eukaryotic RNA processing, including the decapping complex and 3′−5′ poly(A)-specific ribonuclease and the carbon catabolite repressor 4 (CCR4) complex[4]. Aberrant RNAs are also degraded by 5′−3′ XRN exonucleases and the multimeric 3′−5′ exosome complex in cooperation with cofactors for its subcellular function[4].

Evidence indicates that RNA surveillance and PTGS pathways are functionally interconnected through their repression of invasive RNAs and endogenous mRNAs[5–8]. When RNA surveillance is impaired, for instance, S-PTGS and RNA silencing of endogenous genes are induced, suggesting that RNA surveillance restrains PTGS. The production of 21–22 nt siRNAs from exogenous and endogenous protein-coding genes is enhanced in RNA surveillance mutants, indicating that the accumulation of aberrant transcripts due to attenuated RNA surveillance triggers PTGS to generate siRNAs[7,9,10]. However, it is unclear how cells fine-tune RNA surveillance and PTGS.

The ubiquitin–proteasome machinery functions as a protein quality control system for protein degradation and turnover in eukaryotes. The 26S proteasome is an ATP-dependent protease complex that degrades many intracellular proteins in a ubiquitin-dependent manner, including damaged proteins[11]. The proteasome holoenzyme is composed of two major assemblies: the 20S core protease and the 19S regulatory particle[12]. Protein degradation occurs in the central chamber of the 20S core particle, which is assembled from four stacked rings of heteroheptameric α and β subunits[13]. The 19S regulatory particle consists of a base containing six AAA-ATPases (RPT1-6) with four non-ATPase subunits (RPN1, RPN2, RPN10 and RPN13) and a lid composed of at least nine RPN subunits (RPN3, RPN5–9, RPN11, RPN12 and RPN15), responsible for target recognition and proteolytic entry processing[14]. The 26S proteasome complex plays a role in a broad range of biological processes. In plants, the 26S proteasome complex is involved in the regulation of development, defence and chromatin architecture[15]. Mutants for several 26S proteasome subunits show distinct developmental phenotypes and responses to external stimuli[16–18], suggesting that discrete functional specificity of individual subunits may exist. However, the underlying molecular mechanism remains elusive.

[1]Center for Plant Aging Research, Institute for Basic Science, Daegu, Republic of Korea. [2]Department of New Biology, DGIST, Daegu, Republic of Korea. [3]Guangdong Provincial Key Laboratory for Plant Epigenetics, College of Life Sciences and Oceanography, Shenzhen University, Shenzhen, China. [4]Plant Systems Engineering Research Center, Korea Research Institute of Bioscience and Biotechnology, Daejeon, Republic of Korea. *e-mail: yjkim77@ibs.re.kr; jkwak@dgist.ac.kr

Here we show that RPT2a, a subunit of the 26S proteasome complex, promotes siRNA-mediated PTGS against sense transgenes by antagonizing the RQC pathway. We found that green fluorescent protein (GFP) suppression in a genetic system designed for detecting both miRNA- and siRNA-mediated PTGS is de-repressed in *rpt2a* mutants through reduction of transgene-derived siRNA accumulation. The de-repression of GFP expression was also observed in mutants for several other proteasome subunits, but not all, implying that RPT2a confers a specific function to the 26S proteasome complex in S-PTGS. Moreover, RPT2a directly interacted with specific components of the RQC pathway and the protein level was upregulated in *rpt2a* mutants. We provide evidence that cytoplasmic foci enriched with RPT2a are co-localized with siRNA-bodies and granules containing RQC components[5]. Furthermore, the recovered GFP expression in *rpt2a* was suppressed in mutants for the RPT2a-interacting RRP45a, an RQC component. We demonstrate that RPT2a represses the RQC pathway, thereby promoting S-PTGS in a tug of war between RNA surveillance and PTGS.

Results

A reporter system for analysing miRNA- and siRNA-mediated PTGS. To investigate the role of small regulatory RNAs in PTGS, we established a cell type-specific reporter system consisting of the promoter of the stomatal lineage marker gene *TOO MANY MOUTHS* (*TMM*) driving expression of a GFP-luciferase reporter (*GFPLuc*, prey) and the *SUC2* promoter, which is expressed in companion cells of phloem tissue[19], driving expression of an artificial miRNA[20] designed to target *GFPLuc* (amiR-Luc, Orion) (Fig. 1a and Extended Data Fig. 1a,b). In *Arabidopsis thaliana* ecotype Columbia (Col-0) transgenic plants harbouring the *GFPLuc* prey and an empty vector ('prey plants'), GFP fluorescence was observed in early stomatal lineage cells in cotyledons and true leaves in 18 out of 20 independent lines (Fig. 1a and Extended Data Fig. 1b), consistent with the expression pattern of the *TMM* promoter[21]. In contrast, in 28 out of 34 transgenic plants harbouring both the prey and the amiR-Luc Orion, GFP was not detected in cotyledons or true leaves, and only transiently in emerging young leaves (Fig. 1a and Extended Data Fig. 1b). One of the transgenic plants was selected for further study and entitled PORI (prey/Orion).

To determine whether amiR-Luc was responsible for *GFPLuc* repression, we first demonstrated that amiR-Luc is expressed in PORI plants, compared with wild-type and prey plants (Extended Data Fig. 1c). Crossing PORI plants to three mutants defective in miRNA processing and function, *se-1* (*serrate-1*), *hyl1-2* (*hyponastic leaves1-2*) and *ago1-27* resulted in a partial recovery of GFP fluorescence in cotyledons 3 d after germination (DAG) in PORI/*se-1* and PORI/*hyl1-2* followed by a diminution after 4 DAG, compared with PORI plants (Fig. 1b). We also observed partial de-repression of GFP fluorescence in true leaves of the PORI/*se-1* and PORI/*hyl1-2* plants (Fig. 1b), despite significant reduction of amiR-Luc in these mutants (Fig. 1c and Extended Data Fig. 2a). These results raise the possibility that other repression systems may function together with amiR-Luc to silence GFP in PORI plants.

AGO1 is a silencing effector protein acting in both miRNA- and siRNA-mediated PTGS[22,23]. The introduction of the *ago1-27* mutation into PORI plants restored GFP fluorescence in cotyledons and true leaves compared with PORI/*se-1* and PORI/*hyl1-2* (Fig. 1b). This suggests that GFP repression in PORI plants may also be attributable to the action of siRNAs. To address this possibility, we crossed PORI plants to *rdr6-11* and *sgs3-12* mutants defective in siRNA production required for PTGS[24,25]. GFP fluorescence was restored in both PORI/*rdr6-11* and PORI/*sgs3-12* plants (Fig. 1b), indicating that siRNA-mediated PTGS contributes, at least in part, to *GFP* silencing in PORI plants.

Transgene silencing at the post-transcriptional level mainly occurs via 21–22 nt siRNAs, derived from the transgene[26]. Given that GFP fluorescence was restored in the *rdr6-11* and *sgs3-12* mutants, we hypothesized that RDR6-dependent siRNAs may be produced from the *GFPLuc* transgene. To address this idea, we performed small RNA (sRNA) sequencing and found sRNAs mapping to the *GFPLuc* gene in PORI plants (Fig. 1d). The 21 nt sRNAs were most abundant (~70%) with 22 nt RNAs being second most abundant (~20%) (Extended Data Fig. 2b). Quantitative reverse transcription-PCR (qRT–PCR) revealed that accumulation of the 21 and 22 nt sRNAs derived from *GFPLuc* was highly reduced in *rdr6-11* (Fig. 1e), suggesting that these siRNAs are *RDR6* dependent (hereafter referred to as GFPLuc-siRNAs) unlike amiR-Luc, whose production is independent of RDR6 (Fig. 1c and Extended Data Fig. 2a). Treatment of PORI plants with 5-aza-2′-deoxycytidine, an inhibitor of cytosine methylation, did not affect the GFP silencing (Extended Data Fig. 2c) suggesting that transcriptional gene silencing mediated by RNA-dependent DNA methylation (RdDM) is unlikely to affect GFP silencing. GFP expression was not altered in *ago4-6* and *rdr2-2* mutants (Fig. 1b), key components in the RdDM pathway[27,28] and RdDM-dependent 24 nt sRNAs were generated at very low levels compared with 21 and 22 nt siRNAs (Extended Data Fig. 2b). Together, these results indicate that our PORI system can detect both miRNA- and siRNA-mediated PTGS and that siRNA-mediated PTGS mainly contributes to GFP silencing in the PORI plants.

Proteasome subunit RPT2a is required for GFP suppression. A mutant, cs838, isolated while characterizing PORI plants, displayed a serrated leaf phenotype, short height and defects in flower development (Extended Data Fig. 3a) pleiotropic phenotypes that resemble mutants defective in miRNA pathways. To test whether the cs838 mutation is involved in miRNA biogenesis, processing or function, we crossed cs838 to PORI plants. All F2 plants showing the cs838 phenotype recovered GFP fluorescence (Fig. 2a), indicating that the mutated gene in cs838 plays a role in miRNA- and/or siRNA-mediated PTGS. Whole genome sequencing of the cs838 mutant revealed a 72 nt in-frame deletion in the second exon of the *RPT2a* gene encoding a subunit of 26S proteasome complex (Fig. 2b). This mutation results in a 24 amino acid deletion in the AAA-type ATPase core domain that is important for the RPT2a activity[16] (we thus name cs838 *rpt2a-6*; Fig. 2b). The truncated *RPT2a* (*RPT2aΔ72bp*) fused to a C-terminal FLAG epitope and transiently expressed in tobacco was indeed smaller than RPT2a in size (Extended Data Fig. 3b). Since RPT2a is a subunit of the 26S proteasome complex, we tested whether the 72 nt in-frame deletion in RPT2a affects its association in the 26S proteasome complex. Similar to the interaction between RPT2a and RPT4a, RPT2aΔ72bp associated with RPT4a (Extended Data Fig. 3c). *rpt2a-6* is recessive, similar to *rpt2a-2* (ref. [29]; Extended Data Fig. 3d). The *RPT2aΔ72bp* mutation appears to be antimorphic[30] as the GFP expression and morphological phenotypes of PORI/*rpt2a-6* were rescued when *RPT2a* was ectopically expressed from the 35S promoter but not from its native promoter (Extended Data Fig. 3e,f). The introduction of *rpt2a-2* into PORI plants recovered GFP fluorescence similar to PORI/*rpt2a-6* (Fig. 2a). Moreover, crossing PORI/*rpt2a-6* to *rpt2a-2* resulted in no change in GFP fluorescence or morphological phenotypes (Fig. 2a). Thus, RPT2a contributes to GFP silencing in the PORI plants.

RPT2a promotes the production of transgene-derived siRNA. Since RPT2a is a 26S proteasome subunit, we hypothesized that the GFPLuc protein is a direct target of the 26S proteasome, and the recovery of GFP fluorescence in *rpt2a-6* is due to increased accumulation of GFP protein rather than a reduction in PTGS. To test this idea, we examined *GFPLuc* mRNA in PORI and PORI/*rpt2a-6* plants. qRT–PCR revealed that the level of *GFPLuc* transcripts in PORI/*rpt2a-6* was approximately ninefold higher compared with

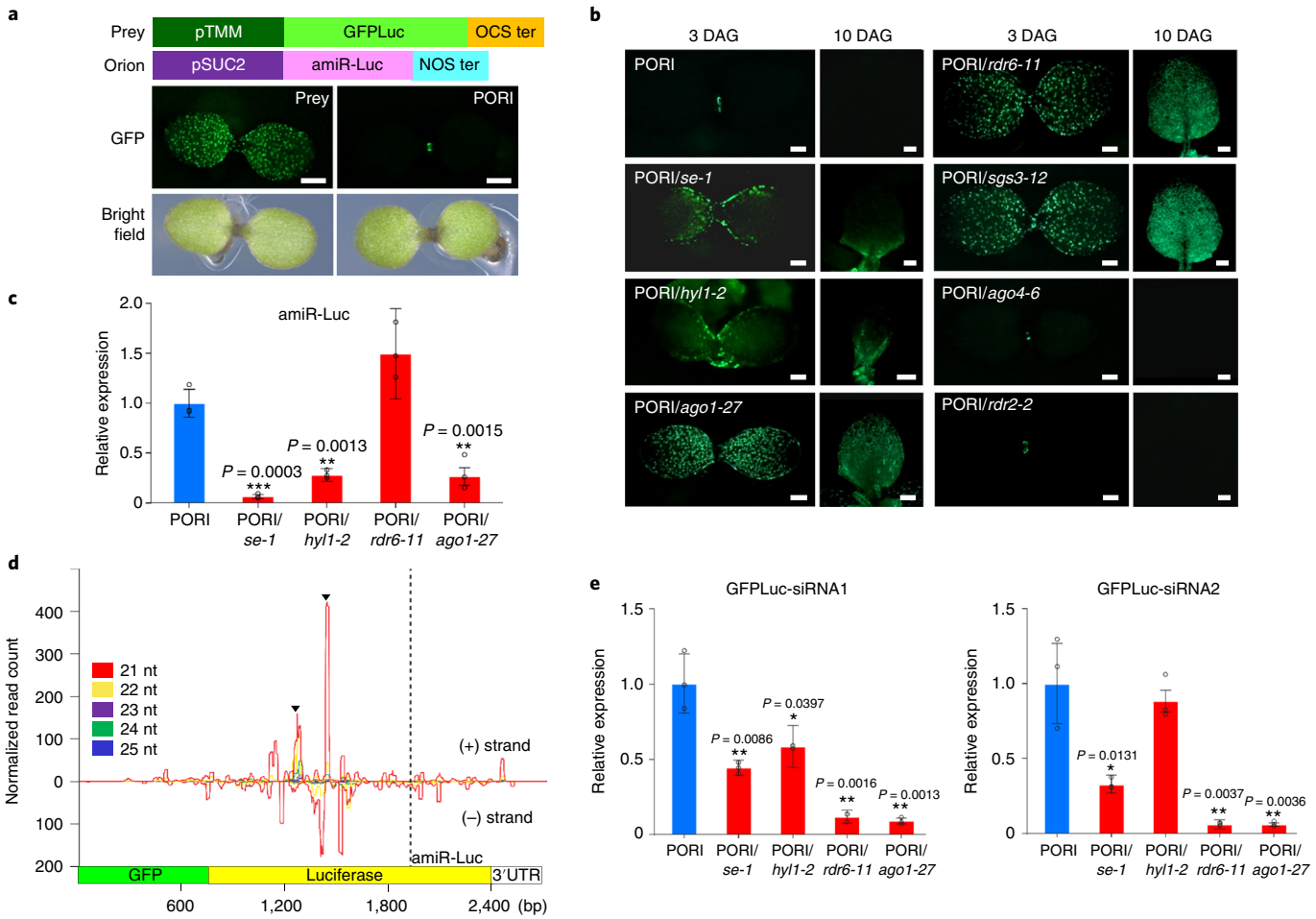

Fig. 1 | *GFPLuc* in PORI plants undergoes miRNA- and siRNA-mediated PTGS. a, A schematic of the prey and Orion constructs (upper) and the GFP expressions of transgenic lines carrying the prey with an empty vector or Orion in cotyledons at 3 DAG (lower). Scale bars, 500 μm. OCS ter, octopine synthase terminator; NOS ter, nopaline synthase terminator. **b**, GFP fluorescence of the PORI and mutants for genes acting in the miRNA or siRNA machinery (cotyledons at 3 DAG or first true leaf at 10 DAG). Scale bars, 300 μm. The segregation analysis of progenies from the genetic crosses is shown in Supplementary Table 1. **c**, qRT-PCR analysis of sRNA showing the relative levels of amiR-Luc in miRNA- or siRNA-deficient mutants. The relative expression values shown were obtained by normalization to that of U6 RNA. **d**, sRNA sequencing analysis of GFPLuc-siRNAs mapped to both strands of *GFPLuc* in PORI plants. The dotted line indicates amiR-Luc-binding sites. Arrowheads represent siRNA sequences used for qRT-PCR to detect GFPLuc-siRNAs. **e**, qRT-PCR analysis of sRNA showing the relative levels of GFPLuc-siRNA in miRNA- or siRNA-deficient mutants. The relative expression values shown were obtained by normalization to that of U6 RNA. Total RNAs were extracted from seedlings at 10 DAG. In **c** and **e**, error bars represent mean ± s.d. calculated from three independent biological repeats. Two-sided Student's *t*-test *P* values: $^{*}P < 0.05$; $^{**}P < 0.01$; $^{***}P < 0.001$.

PORI plants (Extended Data Fig. 4a), suggesting that RPT2a regulates *GFPLuc* at the level of its transcript. To determine whether RPT2a regulates the expression of *TMM* by affecting the *TMM* promoter activity, we examined *TMM* transcript levels and found no increase in *rpt2a-6* (Extended Data Fig. 4b), suggesting that RPT2a does not affect the transcription of *GFPLuc* driven by the *TMM* promoter.

To determine whether RPT2a acts through miRNA- or the siRNA-mediated PTGS to repress *GFPLuc* mRNA levels, we monitored GFP fluorescence in PORI/*rpt2a-6* plants and found that de-repressed GFP fluorescence persisted at a high level in leaves (Fig. 2a and Extended Data Fig. 4c), similar to PORI/*rdr6-11* in which siRNA-mediated PTGS is defective (Fig. 1b and Extended Data Fig. 4c). This result implies that RPT2a functions in siRNA-mediated PTGS rather than miRNA-mediated PTGS. sRNA sequencing in PORI/*rpt2a-6* plants revealed that 21 to 25 nt siRNAs were distributed across the *GFPLuc* region in PORI plants, whereas the siRNAs were dramatically reduced in PORI/*rpt2a-6* plants (Fig. 2c) indicating that RPT2a promotes the production of GFPLuc-siRNAs.

To examine the role of RPT2a in siRNA-mediated PTGS, we used L1 reporter plants in which *β-GLUCURONIDASE* (*GUS*)-derived siRNAs (GUS-siRNAs) mediate S-PTGS of the p35S::GUS transgene[31]. GUS activity in L1/*rpt2a-6* seedlings was much higher compared with that in L1 seedlings (Fig. 2d) and qRT–PCR analysis revealed a significantly higher accumulation of *GUS* mRNAs in L1/*rpt2a-6* seedlings compared with L1 seedlings (Extended Data Fig. 4d). The level of GUS-siRNAs was significantly reduced in the L1/*rpt2a-6* plants compared with the L1 plants (Fig. 2e), indicating that RPT2a promotes the production of transgene-derived siRNAs in S-PTGS. To test whether RPT2a has a role in inverted-repeat PTGS (IR-PTGS)[32], we generated JAP3/*rpt2a-6* plants. The JAP3 photobleaching phenotype, mediated by repeat-derived siRNAs, was not affected by the *rpt2a-6* mutation (Extended Data Fig. 4e). Thus, RPT2a facilitates S-PTGS but not IR-PTGS via the production of transgene-derived siRNAs.

To determine whether the GFP silencing by RPT2a is a general function of the 26S proteasome or a specific function of RPT2a, we analysed GFP fluorescence in PORI plants crossed to mutants for

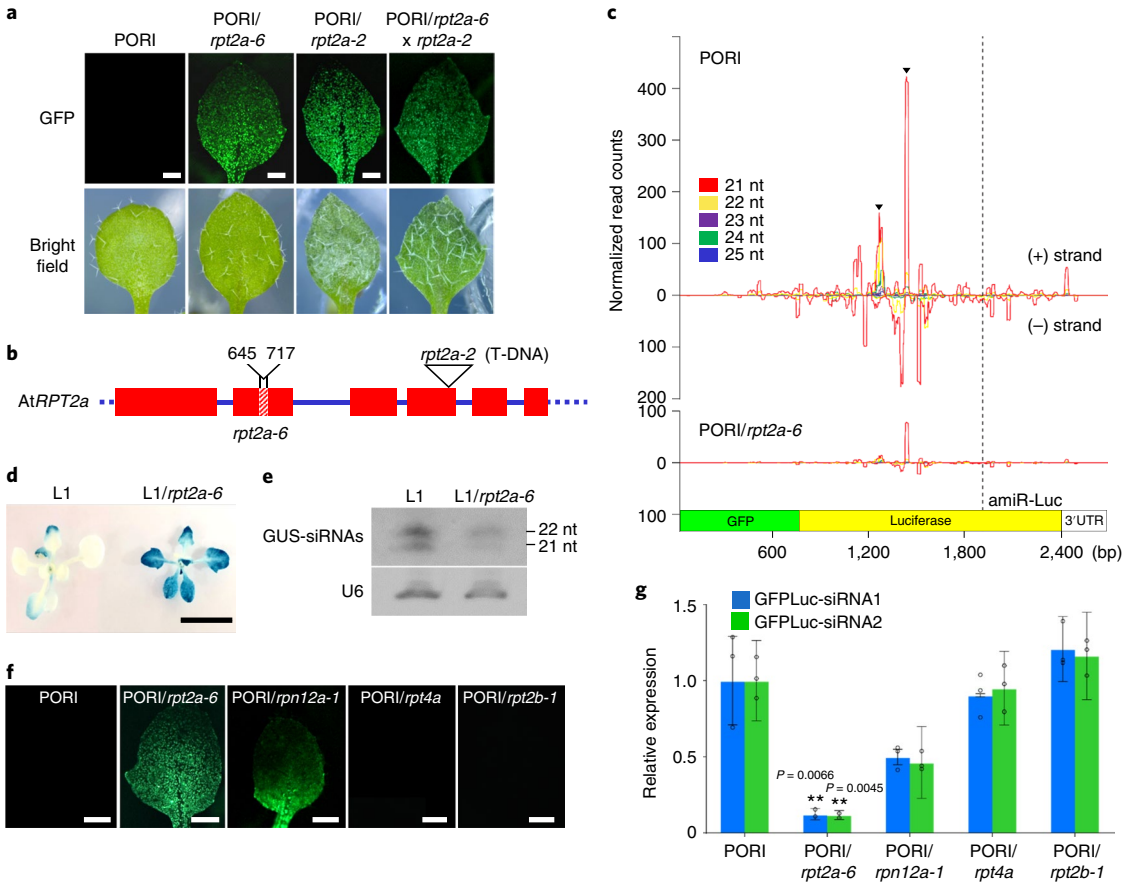

Fig. 2 | RPT2a is required for the production of transgene-derived siRNAs. a, Fluorescence (GFP) and bright-field images of the first true leaves of PORI and PORI/*rpt2a* plants at 10 DAG. Scale bars, 200 μm. The segregation analysis of progenies from the genetic crosses is shown in Supplementary Table 1. **b**, A schematic of the *RPT2a* structure showing the positions of 72 bp deletion (645th to 717th nucleotides from the start codon) in *rpt2a-6* and the T-DNA insertion in *rpt2a-2*. **c**, sRNA sequencing analysis of GFPLuc-siRNAs mapped to both strands of *GFPLuc* in PORI and PORI/*rpt2a-6* plants. The dotted line indicates amiR-Luc binding sites. Total RNAs extracted from seedlings at 10 DAG were used for sRNA sequencing analysis. **d**, Histochemical GUS staining of L1 and L1/*rpt2a-6* seedlings. Scale bar, 1 cm. At least 15 independent plants showed similar results. **e**, Northern blot analysis shows the accumulation of GUS-siRNAs in L1 and L1/*rpt2a-6* plants. U6 RNA was used as a loading control. The experiment was independently repeated two times with similar results. **f**, GFP fluorescence in the first true leaves of PORI and PORI/proteasome subunit mutants. Scale bars, 500 μm. The segregation analysis of progenies from the genetic crosses is shown in Supplementary Table 1. **g**, qRT-PCR analysis of GFPLuc-siRNAs in PORI and PORI/proteasome subunit mutants. Error bars represent mean ± s.d. from three independent biological replicates. Two-sided Student's *t*-test *P* values: $^{*}P < 0.05$; $^{**}P < 0.01$.

other 26S proteasome subunit genes, including *RPN12a* and *RPT4a*. In the *rpn12a* mutant background, GFP fluorescence was partially restored, but remained relatively weak compared with *rpt2a-6* (Fig. 2f), and the levels of the GFPLuc-siRNAs were much lower compared with PORI plants but higher compared with PORI/*rpt2a-6* plants (Fig. 2g). By contrast, the *rpt4a* mutation did not impact GFP fluorescence or GFPLuc-siRNA levels (Fig. 2f,g). Crossing a null mutant for *RPT2b*, the closest homologue of *RPT2a* (ref. [16]), into PORI (PORI/*rpt2b-1*) had no effect on GFP fluorescence or GFPLuc-siRNA levels, compared with the PORI plants (Fig. 2f,g). Next, we treated PORI plants with the proteasome inhibitor MG132 to further examine the role of the 26S proteasome for S-PTGS. The PORI plants treated with MG132 showed stronger GFP fluorescence compared with the mock-treated plants (Extended Data Fig. 4f). These results imply that the 26S proteasome complex is required for S-PTGS and that RPT2a plays a central role in S-PTGS.

Many components are shared between endogenous sRNA biogenesis and foreign RNA-derived sRNA biogenesis in PTGS[33,34]. Our results show that several key components of the endogenous sRNA biogenesis pathway, such as RDR6, SGS3, AGO1, HYL1 and SE, are required for GFP silencing in PORI plants (Fig. 1b). To investigate whether RPT2a plays a role in endogenous sRNA biogenesis and consequently regulates the production of GFPLuc-siRNAs, we analysed endogenous sRNA accumulation in PORI/*rpt2a-6*. The accumulation of miRNAs, *trans*-acting siRNAs (ta-siRNAs), and heterochromatic siRNAs (hc-siRNAs) were largely unchanged, compared with the PORI plants (Fig. 3a–c), indicating that RPT2a is not involved in endogenous sRNA production and likely acts in a different cellular pathway.

RPT2a directly represses a subset of RQC components. RQC is a key plant defence mechanism against invasion of foreign RNA and accumulation of aberrant endogenous RNAs[1]. The RQC pathway competes with PTGS: target RNAs are rapidly degraded by components of RQC, preventing their conversion into double-stranded RNAs, which are required for triggering PTGS[1]. Given that RPT2a does not affect the biogenesis of siRNAs, we hypothesized that RPT2a may antagonize the RQC machinery, thereby promoting S-PTGS in PORI plants. Since the 26S proteasome complex degrades target proteins through physical interactions, we hypothesized that RPT2a could repress RQC components by associating directly with them. Thus, we performed a yeast two-hybrid assay and tested

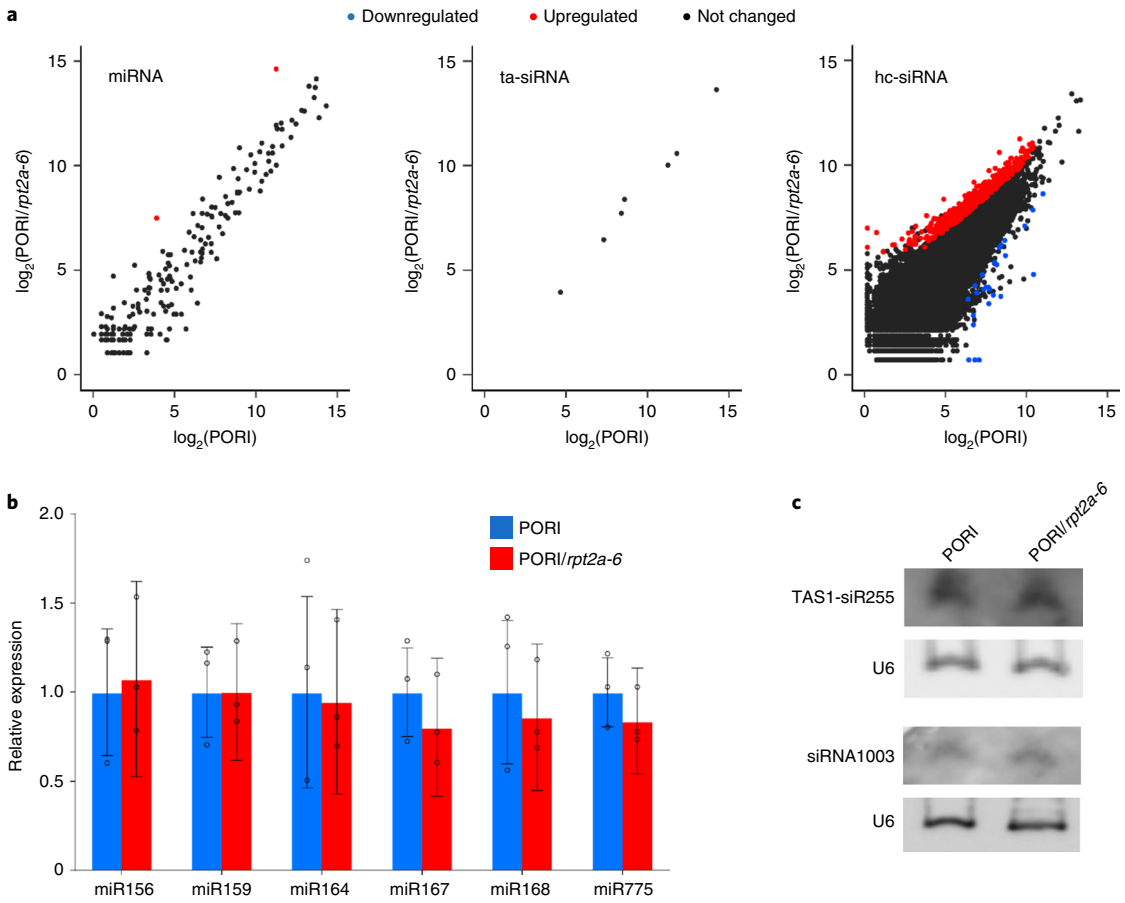

Fig. 3 | Expression of endogenous miRNA and siRNA are not altered in *rpt2a-6*. **a**, Scatter plot analyses of miRNA, ta-siRNA and hc-siRNA between PORI and PORI/*rpt2a-6*. Red dot, ratio > 2; blue dot, ratio < 0.5; black dot, 0.5 < ratio < 2. **b**, Validation of sRNA sequencing results by qRT–PCR analysis of miR156, miR159, miR164, miR167, miR168 and miR775 in in PORI and PORI/*rpt2a-6*. Error bars represent mean ± s.d. from three independent biological replicates. **c**, Northern blot analysis of ta-siRNAs and an hc-siRNA in PORI and PORI/*rpt2a-6*. U6 RNA was used as an internal control. The experiment was independently repeated three times with similar results.

several components in the RQC pathway, including decapping proteins (DCP1, DCP2), a 5′−3′ exonuclease (XRN4) and 3′−5′ exonucleases (RRP4, RRP41, CER7, RRP45a). DCP2, RRP41 and RRP45a physically interacted with RPT2a (Fig. 4a). To further validate the interactions, we performed co-immunoprecipitation experiments and found that the interaction between RPT2a and DCP2/RRP41/RRP45a was specific. mCherry, VPS9a (VACUOLAR SORTING PROTEIN 9; AT3G19770; randomly selected) and DCP1 were used as negative controls and did not co-immunoprecipitate with RPT2a (Extended Data Fig. 5a,b). By contrast, RRP4 co-immunoprecipitated with RPT2a (Extended Data Fig. 5c). Since RRP4 is also subunit of the exosome complex, we reason that RRP4 could be pulled down with the RRP45a-containing complex associated with RPT2a.

To determine whether the physical interaction of RPT2a with the RQC proteins contributes to the regulation of the proteins in vivo, we examined DCP2 and RRP45 protein levels in *rpt2a-6*. We crossed *rpt2a-6* plants to transgenic plants harbouring *pDCP2::DCP2-GFP* that fully rescued the phenotype of *dcp2* (*dcp2-1*/DCP2-GFP)[35] and found that the DCP2 protein level was elevated in *rpt2a-6* compared with wild-type plants (Fig. 4c, left) without any change at the transcript level of *DCP2* (Extended Data Fig. 6a). The MG132 treatment resulted in a higher level of DCP2 protein, implying that DCP2 protein is regulated through the interaction with RPT2a of the 26S proteasome (Fig. 4c, right). There were no clear differences in the levels of RRP45a protein in either a wild-type or *rpt2a-6* background (Extended Data Fig. 6b). We do not exclude a possibility that RPT2a may repress RRP45a under certain cellular circumstances.

RPT2a localizes with speckles containing RQC and PTGS components. Given that RPT2a interacts with a subset of RQC components and modulates siRNA-mediated PTGS, we assessed the subcellular localization of RPT2a, RPT2a-interacting RQC components (DCP2, RRP41 and RRP45a) and SGS3 (a marker for the siRNA-body, which colocalizes with RDR6) using transient expression in tobacco. DCP2 localizes to cytoplasmic speckles called P-bodies and SGS3 to siRNA-bodies. P-bodies and siRNA-bodies are dynamically linked in the cell[5]. When RPT2a, DCP2 and SGS3 were transiently expressed together, most of the RPT2a-GFP speckles were localized to the place where P-bodies and siRNA-bodies interact with each other (Fig. 4d). RPT2a-GFP speckles appeared to be co-localized to siRNA-bodies in distinct forms (Fig. 4d and Extended Data Fig. 7), whereas most of the RPT2a-localized speckles entirely overlapped with RRP41-mCherry and RRP45a-mCherry at spots where siRNA-bodies were localized (Fig. 4d).

RQC components RRP41 and RRP45a are known to be localized both in the nucleus and the cytoplasm but RRP41- and RRP45a-enriched foci have not been observed[36,37]. When RPT2a, RRP41 and RRP45a were individually expressed in the absence of SGS3, they were found in the nucleus and the cytoplasm (Extended Data Fig. 7a), and no RPT2a- or RRP41/RRP45a-localized speckles were observed (Extended Data Fig. 7b–d). We found that only in the

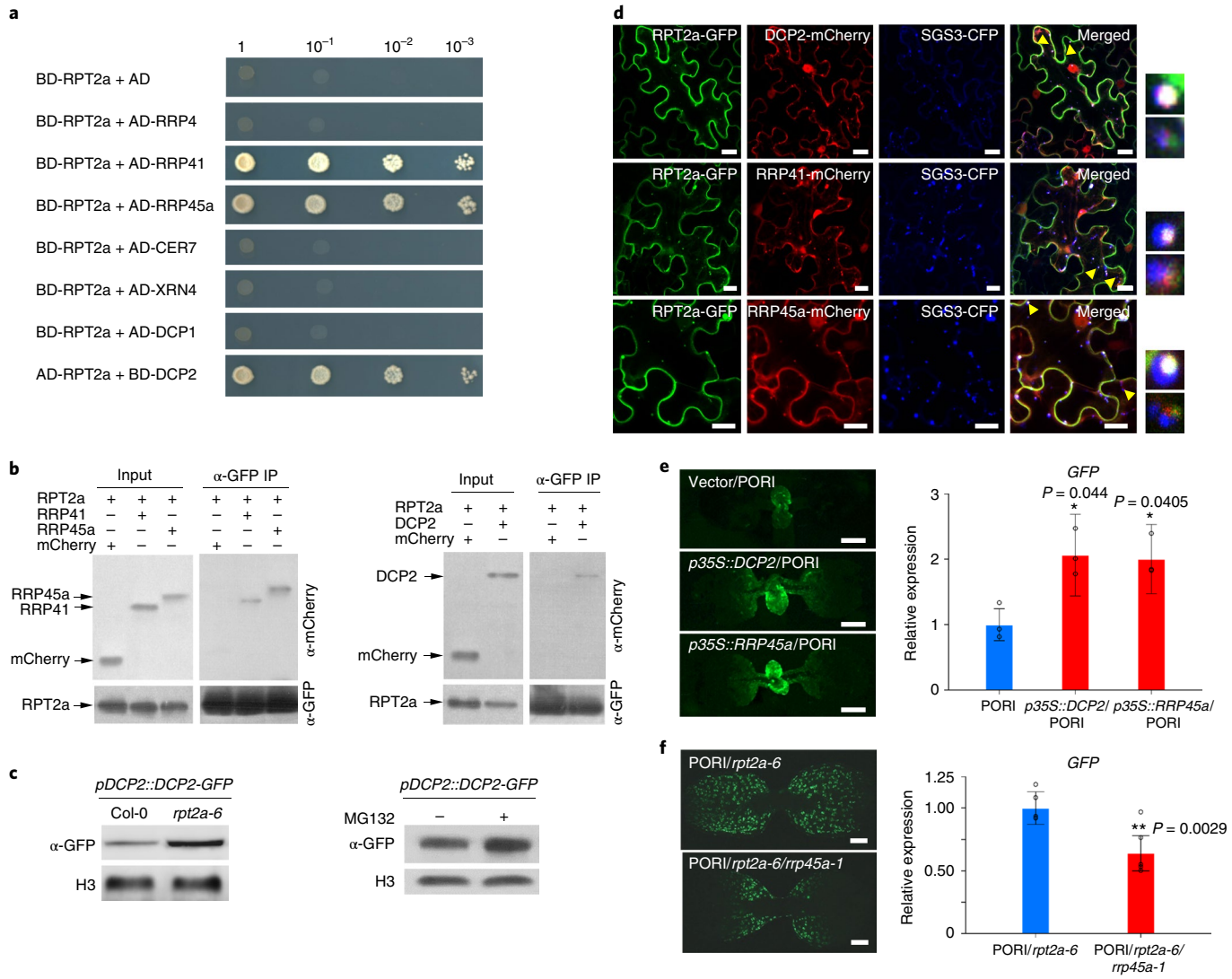

Fig. 4 | A subset of RQC components is targets of RPT2a in vivo. a, Yeast two-hybrid assays show the physical interaction between RQC components (RRP41, RRP45a, DCP2) and RPT2a. AD, activation domain; BD, binding domain. For the serial dilution analysis, yeast cells were diluted to 1, 10^{-1}, 10^{-2} and 10^{-3}. At least three independent colonies for each interaction were tested and showed similar results. **b**, Co-immunoprecipitation analysis validates the interaction between RPT2a and DCP2, RRP41 and RRP45a. RPT2a-GFP, RRP41-mCherry, RRP45a-mCherry and DCP2-mCherry were expressed in tobacco plants expressing SGS3-cyan fluorescent protein (CFP). The experiment was independently repeated at least three times with similar results. **c**, Western blot analysis of DCP2 protein in wild-type and *rpt2a-6* plants (left), and in the absence and presence of MG132 (right). Total protein was extracted from plants harbouring the DCP2-GFP construct at 10 DAG. Histone 3 was used as a loading control. The experiment was independently repeated at least three times with similar results. **d**, Subcellular localization of RPT2a, SGS3 and RQC proteins. The proteins were transiently expressed in tobacco leaves. The yellow arrowheads indicate co-localized granules of RPT2a and SGS3 in combination with DCP2 (top row), RRP41 (middle row) or RRP45a (bottom row). Enlarged views are shown in the small boxes on the right side. Scale bars, 20 μm. The experiment was independently repeated at least five times with similar results. **e**, The GFP fluorescence (left) and the expression level of *GFP* in the control, *p35S::DCP2*/PORI and *p35S::RRP45a*/PORI plants (right). The relative expression values were obtained by normalization to *UBQ5*. Three independent transgenic plants were analysed for each construct and showed consistent results. **f**, GFP fluorescence (left) and the expression levels of *GFP* in PORI/*rpt2a-6* and PORI/*rpt2a-6/rrp45a-1* plants (right). In **e** and **f**, the relative expression values were obtained by normalization to *UBQ5*. Error bars represent mean ± s.d. calculated from five biological replicates. Scale bars, 300 μm. Two-sided Student's *t*-test *P* values: $^{*}P < 0.05$; $^{**}P < 0.01$.

presence of SGS3-enriched siRNA-bodies did RPT2a- or RRP41/RRP45a-localized speckles form, which were closely interfaced with the siRNA-bodies (Extended Data Fig. 7b–d), suggesting that SGS3 may affect the subcellular localization of RPT2a, RRP41 and RRP45a. Together, these results further support that a subset of RQC components are targets of RPT2a and imply a functional link between RPT2a, RQC and PTGS.

RPT2a promotes S-PTGS via RQC machinery. To test whether RPT2a promotes GFP silencing by associating with RQC components in PORI plants, we expressed *DCP2* and *RRP45a* in PORI plants and analysed GFP fluorescence. *DCP2*- and *RRP45a*-overexpression plants showed prolonged and increased GFP expression, together with increased *GFPLuc* transcript levels, compared with PORI plants harbouring an empty vector (Fig. 4e and Extended Data Fig. 8), suggesting that *DCP2* and *RRP45a* contribute to triggering S-PTGS in PORI plants. We also tested whether regulation of the RQC components by RPT2a is necessary for GFP silencing in the PORI plants, focusing on *RRP45a*, as the null alleles of *DCP2* and *RRP41* are lethal[37,38]. We crossed PORI/*rpt2a-6*

plants to loss-of-function mutants for *RRP45a* and observed that the GFP fluorescence, and its transcript levels were indeed reduced in PORI/*rpt2a-6/rrp45a*-1 compared with PORI/*rpt2a-6* (Fig. 4f), implying that RPT2a-mediated GFP suppression requires RRP45a in the PORI plants.

Since the GFP expression in the 35S::DCP2/PORI and 35S::RRP45a/PORI plants was much lower compared with the PORI/*rpt2a-6* plants and the PORI/*rpt2a-6*/*rrp45a-1* plants did not display near-complete GFP silencing, it is presumed that RPT2a represses both decapping and 3′ to 5′ RNA degradation, thereby resulting in effective control of GFP silencing in the PORI plants. Together, these results indicate that RPT2a represses the RQC machinery, resulting in the promotion of S-PTGS in the PORI plants.

RQC siRNAs (rqc-siRNAs) are a new class of RDR6-dependent 21 nt siRNAs and generated from hundreds of endogenous mRNAs in the decapping mutant *dcp2* (ref. [5]). Similarly, the impairment in the 5′ to 3′ and/or 3′ to 5′ RNA degradation pathway provokes the production of siRNAs from protein-coding genes, which resemble rqc-siRNAs[7,39]. It is proposed that the RQC machinery restrains PTGS by preventing the production of rqc-siRNAs to avoid unintended entry of aberrant RNAs of endogenous mRNAs into PTGS. Since RPT2a represses the RQC pathway, we tested whether RPT2a affects the production of endogenous gene-derived sRNAs such as rqc-siRNAs. We found 816 loci mapped to genes produce 21 nt sRNAs, and 15 of the loci showed reduced level in *rpt2a-6* (Supplementary Table 7), suggesting that RPT2a barely affects the production of endogenous gene-derived sRNAs including rqc-siRNAs.

Discussion

miRNAs and siRNAs are small regulatory RNAs that can act locally and at a distance to control target gene expression, which is essential for development, environmental fitness and genome defence in plants. In the present study, we have developed a dual reporter system (PORI) that allows the monitoring of miRNA- and siRNA-mediated PTGS. Utilizing this reporter system, we found that the proteasome subunit RPT2a promotes the production of GFP-siRNAs by antagonizing the RQC pathway, thereby contributing to the PTGS of the *GFPLuc* reporter in PORI plants.

GFPLuc-siRNAs regulate *GFPLuc* (Fig. 1a,e), raising the question as to what evokes the production of GFPLuc-siRNAs in PORI plants. One possibility is that amiR-Luc-mediated GFPLuc cleavage products trigger the generation of GFPLuc-siRNAs. The cleavage products of a subset of miRNA target genes are known to serve as substrates for RDR6, resulting in the production of siRNAs[7,40], although the mechanism for substrate selectivity is unclear. In PORI plants, amiR-Luc cleaves *GFPLuc* and the cleavage products of *GFPLuc* may have served as substrates for RDR6, which in turn could trigger siRNA production. Several observations made in our study support this possibility. First, GFP silencing in newly developing leaves appears to be spatiotemporally correlated with the activity of the *SUC2* promoter that drives amiR-Luc expression in a cell type-specific manner (Extended Data Fig. 1b), suggesting that amiR-Luc activity is required during the initial stages of GFP silencing. Second, GFPLuc-siRNAs are predominantly produced from the 5′ cleavage product (Fig. 2c). A subset of endogenous miRNA target genes produce RDR6-dependent secondary siRNAs (rqc-siRNAs or coding transcript-derived siRNAs), mainly from 5′ cleavage products[7,40]. Third, GFP-siRNA accumulation is reduced in *se-1* and *hyl1-2* mutants (Fig. 1e), in which miRNA biogenesis is largely abolished. In addition, while GFP expression was suppressed in most of the T1 transgenic lines carrying the prey and amiR-Luc (28 out of 34), the majority of T1 transgenic lines carrying the prey and the empty vector (18 out of 20) showed the expected GFP fluorescence driven from the *TMM* promoter (Extended Data Fig. 1b). These results imply that amiR-Luc is required for GFPLuc silencing in PORI plants. In this scenario, we assume that amiR-Luc-mediated *GFPLuc* cleavage products generate secondary siRNAs, mainly from the 5′ cleavage product region, resulting in further amplification of the systemic silencing signal for *GFPLuc*. However, we cannot rule out the possibility that aberrant transcripts of the *TMM* promoter-driven *GFPLuc* accumulate to a point beyond the capacity of RQC to degrade them, resulting in GFPLuc undergoing PTGS to generate siRNAs. Further genetic and biochemical studies will be necessary to address this intriguing point.

Several lines of evidence indicate that the RQC pathway antagonizes PTGS, preventing the potentially indiscriminate degradation of endogenous or exogenous RNAs[1]. However, the molecular mechanism(s) underlying the mutual regulation of these two pathways is largely unknown. Here we have shown that RPT2a is a negative regulator of the RQC pathway by directly promoting the protein degradation of a subset of RQC components. Thus, RPT2a reinforces PTGS, leading to enhanced GFP silencing in the PORI plants. The subcellular localization of RPT2a further supports this idea. RPT2a speckles associated with siRNA-bodies and RNA-processing granules where DCP2 (P-bodies) or RRPs were localized (Fig. 4d), with RPT2a speckles mostly overlapping with P-bodies or RRPs granules, and RPT2a speckles and siRNA-bodies localized in close proximity but in clearly distinct granules (Fig. 4d). Furthermore, studies have shown that RNA-turnover factors are degraded in a proteasome-dependent manner[41,42]. P-bodies are enlarged in 26S proteasome yeast mutants, *pre4-2* and *ump1-2* (ref. [43]), supporting an interplay between proteasomes and P-bodies. It has been also suggested that the abundance of P-body-targeted RNAs may be affected due to the altered P-body activity in those mutants[43]. Since various RNA granules are found to associate with one another in both animals and plants and it is hypothesized that RNAs and their interacting proteins could shuttle between different RNA granules[5], we speculate that in the three-way association between RPT2a speckles, siRNA-bodies and RQC component-enriched bodies, RPT2a directly regulates the level of RQC components. This could ultimately control the partitioning of RNA substrates between RNA silencing and RNA surveillance mechanisms, by which RNAs surplus to RQC capacity would be trafficked into siRNA-bodies, triggering PTGS.

We detected RPT2a- and RRP41/RRP45a-enriched speckles only in the presence of ectopically expressed *SGS3* (Fig. 4d and Extended Data Fig. 7), suggesting that SGS3 is involved in translocating these proteins into proximity of the siRNA-bodies, where PTGS occurs. These results imply that direct regulation of the RQC pathway by RPT2a can be induced when PTGS occurs. Exosome cofactors, such as Ski proteins, are not known to localize to P-bodies in yeast[44]. In contrast, other exosome subunits localize to different subcellular location, including the nucleus, nuclear foci, cytoplasm, cytoplasmic foci and the plasma membrane[45]. One possible explanation is that such exosome subunits may have dynamic subcellular locations that relate to their function in response to internal and external stimuli. In line with this, the protein level of RRP45a was not changed in *rpt2a-6* (Extended Data Fig. 6b) and we speculate that RPT2a represses RRP45a in the cells where PTGS occurs, which is likely to limit an observation of direct repression of RRP45a by RPT2a.

The 26S proteasome holoenzyme degrades regulatory and misfolded proteins to maintain protein homeostasis, and its function has been implicated in a variety of cellular processes[46]. The functional specificity of individual subunits has been recognized in the yeast system[47], with loss-of-function mutants of the 26S proteasome complex in plants showing either similar or distinct developmental defects[15–18]. In addition, individual 26S proteasome subunits exhibit both common and specific responses to environmental stress[48,49]. Other proteasome subunits including RPN12a are also required for the transgene silencing in the PORI plants (Fig. 2f). In addition, the

proteasome inhibitor MG132 treatment restored the GFP expression in the PORI plants (Extended Data Fig. 4f) and inhibited the degradation of DCP2 protein (Fig. 4c), suggesting a requirement of the RPT2a-containing 26S proteasome complex in S-PTGS. Only RPT2a/b, RPT5a/b and RPN8a specifically bind plastid proteins (LTA2 and/or PDH Ea), which are degraded by the 26S proteasome, among 21 tested RPT or RPN subunits in *Arabidopsis*[50]. Therefore, it is possible that in the 26S proteasome holoenzyme RPT2a specifically recognizes substrates DCP2, RRP41 and RRP45a proteins and plays a predominant role in their degradation among RPTs, thereby enforcing PTGS. Alternatively, the plant proteasome complex may exist in structurally dynamic conformations where RPT2a assembles with distinct subunits that promote its proteolytic activity.

The ubiquitin–proteasome system regulates an array of biological processes in plants[15]. Our results point to the direct regulation of a subset of RQC components and, therefore, S-PTGS, by RPT2a, linking the 26S proteasome system to the S-PTGS pathway. This implies that proteasome-mediated selective protein degradation contributes to the fine-tuning of a much broader range of biological processes than previously suspected. In plants, RQC is considered to be the first line of defence against aberrant RNAs, and PTGS is triggered to remove aberrant RNAs when the RQC pathway is compromised. Our results suggest the existence of an additional regulatory layer that favours PTGS in the routing of aberrant RNAs between RQC and PTGS. Because RPT2a does not affect the production of endogenous sRNAs, the cell may actively suppress the RQC pathway using post-transcriptional mechanisms, such as the 26S proteasome complex, to enhance PTGS as a dominant defence mechanism against foreign RNAs.

Methods

Plant materials and growth conditions. *Arabidopsis thaliana* ecotype Columbia (Col-0) was used for all experiments. Plants were grown on 1/2 Murashige and Skoog (MS) media or soil at 22 °C under long-day conditions (16 h light/8 h dark). *dcp2-1*/DCP2-GFP[35], RRP41-myc[51], L1[31] and JAP3[32] transgenic lines were previously described. Transfer DNA (T-DNA) insertion lines for proteasome subunit genes were obtained from the Arabidopsis Biological Resource Center (ABRC) (*rpt2a-2*: SALK_005596; *rpn12a-1*: SALK_134934; *rpt2b-1*: SALK_043450; *rpt4a*: SALK_052372). Segregation analysis of progenies from the genetic crosses is shown in Supplementary Table 1.

Plasmid construction. The plasmids were constructed using the Gateway system. Detailed information is listed in Supplementary Table 2.

RNA extraction and qRT–PCR. Total RNAs were extracted using TRIzol reagent (Invitrogen) and purified with the Quick-RNA Miniprep Kit (Zymo Research). First strand complementary DNA was synthesized from 1 μg of DNase I-treated total RNA using the RNA to cDNA EcoDry Premix (Oligo dT) kit (Clontech) according to the manufacturer's instructions. qRT–PCR was performed using a Bio-Rad CFX 384 Real-Time System (Bio-Rad) with the iQ SYBR Green Supermix (Bio-Rad) according to the manufacturer's instructions. The gene-specific primers used for PCR are listed in Supplementary Table 3.

Whole genome sequencing and analysis. A DNA library was prepared according to the Illumina Truseq Nano DNA Library prep protocol. For sample library preparation, 0.1 μg of high-molecular-weight genomic DNA (for a 350 bp insert size) was randomly sheared to yield DNA fragments using the Covaris S2 system. The fragments were blunt-ended, phosphorylated and a single 'A' nucleotide was added to the 3′ ends of the fragments in preparation for ligation to an adapter with a single-base 'T' overhang. Adapter ligation at both ends of the genomic DNA fragment conferred different sequences at the 5′ and 3′ ends of each strand in the genomic fragment. The ligated DNA was PCR amplified to enrich for fragments with adapters on both ends. The quality of the amplified libraries was verified by capillary electrophoresis (Bioanalyzer, Agilent). The library was clustered on the Illumina cBOT station and sequenced paired-end for 101 cycles on the HiSeq 2500 sequencer according to the Illumina cluster and sequencing protocols.

After a quality control check on the raw read sequences using FastQC, low-quality bases were trimmed from the reads by using sickle v1.31 with the default parameters including a Phred cut-off of 20 (https://github.com/najoshi/sickle). We then mapped the remaining reads to TAIR10 genome assembly by using BWA v0.7.12[52] with the default parameters, and removed PCR duplicates from the aligned reads by using Picard MarkDuplicates v1.119 (http://broadinstitute.github.io/picard/). Only uniquely mapped reads from the BAM files were subjected to local realignment around insertions and deletions (indels) by using the Genome Analysis Toolkit 3.5 (GATK) IndelRealigner[53] with the default parameters and known germline variations from Ensembl database (http://plants.ensembl.org), followed by base quality score recalibration by using the GATK BaseRecalibrator. For each sample, the GATK HaplotypeCaller and GenotypeGVCFs extracted single nucleotide polymorphisms (SNPs) and indels with Phred-scaled confidence > 30 and merged the variant calling files of the individual samples into a single one. Finally, the SNP and indels were filtered by applying the GATK VariantFiltration with the following parameters: for SNPs, QualByDepth (QD) < 2, RMSMappingQuality (MQ) < 40, FisherStrand (FS) > 60, HaplotypeScore > 13, MappingQualityRankSumTest (MQRankSum) < −12.5, and ReadPosRankSumTest (ReadPosRankSum) < −8; and for indels, QD < 2, FS > 200 and ReadPosRankSum < 20.

sRNA sequencing library construction and data analysis. For sample library preparation, total RNAs were isolated from ten-day-old seedlings using Qiagen RNeasy mini Kit. The RNA integrity number (RIN) of each sample was measured using the Agilent Technologies 2100 BioAnalyzer, and RINs for all the samples were larger than 8. After gel electrophoresis of total RNA by TBE-urea PAGE, sRNAs were purified from the excised gel slices. sRNA samples were converted to DNA libraries using the NEBNext Multiplex Small RNA Library Prep Set for Illumina (New England Biolabs), following the manufacturer's protocol. Briefly, 5′ and 3′ adapters were ligated the purified sRNA, followed by the reverse transcription and incorporation of index tags by PCR. The products of this RT–PCR were isolated using 3% Agarose gel of the Sage Pippin Prep, and the size selection of 145–160 bp fraction was performed. The cDNA library samples were sequenced using the Illumina Hiseq2500 system, generating 50 bp single-end reads.

For the data analysis, we first checked the quality of raw read sequences for each sample by FastQC v0.11.2 (Babraham Bioinformatics) and performed the alignment of the read sequences by pRNASeqTools pipeline. (https://github.com/grubbybio/pRNASeqTools). Briefly, we trimmed the adapter sequence ('AGATCGGAAGAGCACACGTCT') from the reads by using Cutadapter v1.9.1[54]. The remaining reads were then aligned to the *A. thaliana* genome (TAIR10) by using ShortStack v3.4 with the default parameters[55]. The reads mapped to the annotated miRNA loci (no mismatches and at most 1 nt shift allowed) were identified as miRNA reads, and the number of the miRNA reads was calculated as the abundance of each miRNA loci. Differential expression analysis of miRNAs was conducted by using R package 'DESeq2'[56] and differentially expressed miRNAs were identified as the ones with their absolute values of $\log_2$-fold-change > 1 and false discovery rates (FDR) < 0.05 (Supplementary Tables 4–6). For differential expression analysis of endogenous gene-derived siRNAs, EdgeR was used to normalize expression levels[57] and identify statistically significant differentially expressed siRNA loci (FDR < 0.05 and fold-change > 2). Then gene expression levels were normalized and differentially expressed genes (DEGs) were calculated with the cut-off of fold-change > 2 (for hyper DEGs) or fold-change < 0.5 (for hypo-DEGs), and $P < 0.05$ using EdgeR. P values were adjusted via the Benjamini–Hochberg method[58] (Supplementary Table 7).

For the transgene analysis, the trimmed reads were aligned to the GFPLuc sequence (Clontech) by using Bowtie v1.1.2 (ref. [59]) with no mismatches and all possible multiple alignments allowed. Among the aligned reads, we then selected the reads with 20 to 25 nt in length, and classified them into two groups based on the orientation of the reads (forward and reverse complement).

Western blot analysis. Floral buds or seedlings were homogenized and extracted with 1 × SDS sample buffer (50 mM Tris-HCl, pH 6.8, 2% SDS, 10% glycerol, 1% β-mercaptoethanol, 12.5 mM EDTA and 0.02 % bromophenol blue). Total protein was loaded on 10% (w/v) SDS–PAGE gel and transferred to Hybond-C Extra membrane (GE Healthcare). The membranes were probed with the anti-c-Myc-HRP (1:4,000 v/v, Abcam, ab19312), anti-eGFP (1:1,000 v/v, Pierce, CAB4211), anti-FLAG M2-peroxidase (HRP) (1:3,000 v/v, Sigma, A8592) and anti-histone H3 (1:10,000 v/v, Abcam, ab1791). The signal was detected with Supersignal West Pico Chemiluminescent Substrate (Thermo-Fisher Scientific) and scanned using ImageQuant LAS 4000 (GE Healthcare Life Sciences).

Analysis of sRNA accumulation. The miScript PCR System was used to validate the accumulation level of miRNA and siRNA. One microgram of DNase I-treated total RNA was synthesized from using miScript II RT Kit (Qiagen) according to the manufacturer's instructions. Quantitative miRNA and siRNA real-time RT–PCR was performed with the miScript II SYBR Green PCR Kit (Qiagen) using 10x universal primer and sRNA-specific primers. The gene-specific primers used for PCR are listed in Supplementary Table 3.

For sRNA northern blot analysis, total RNA (10 μg for miRNAs and 30 μg for siRNAs) was denatured at 70 °C for 10 min. Denatured RNA was separated in 15% denatured polyacrylamide gels and subsequently transferred onto Hybond-N^+ membrane. The membranes were pre-hybridized using ULTRAhyb Ultrasensitive Hybridization Buffer (Applied Biosystems) for 1 h and hybridized overnight at 42 °C with 5′ end biotin-labelled probes. (For the detection of GUS-siRNAs, two probes, GUS-siRNA1-AS and GUS-siRNA2-AS, were mixed[60].) After washing with 2 × SSC, 0.1% SDS and 0.1 × SSC, 0.1% SDS, the signals were detected using

a Chemiluminescent Nucleic Acid Detection Module Kit (Thermo Scientific) and scanned using an ImageQuant LAS 4000 (GE Healthcare Life Sciences).

Yeast two-hybrid assay. The activation domain and binding domain plasmids were co-transformed into *Saccharomyces cerevisiae* AH109 cells. Yeast transformants were grown on dropout-Leu-Trp plates for the selection and selected yeast cells were spotted onto dropout-Leu-Trp-His-Ade plates to test protein–protein interactions.

Tobacco transient expression and co-immuoprecipitation. Cultured Agrobacteria harbouring *p35S::RPT2a-GFP* and *p35S::RRP41-mCherry*, *p35S::RRP45a-mCherry*, *p35S::DCP2-mCherry* and *p35S::mCherry* were resuspended in infiltration buffer (500 mM MES pH 5.6, 500 mM $MgSO_4$, 100 mM acetosyringone) with P19. The leaves were collected after 2 d, and total protein was extracted in IP buffer (50 mM Tris·HCl pH 8.0, 150 mM NaCl, 10% glycerol, 0.5 Mm DTT, 5 mM $MgCl_2$, 0.1% NP40, EDTA-free protease inhibitor cocktail Tablets (Roche)). The protein extract was incubated with GFP-Trap_A (ChromoTek), anti-GFP conjugated agarose beads. After 2 h incubation at 4 °C, the beads were washed three times with washing buffer (50 mM Tris·HCl pH 8.0, 150 mM NaCl, 10% glycerol, 0.5 Mm DTT, 5 mM $MgCl_2$). Anti-eGFP (1:1,000 v/v, Pierce, CAB4211) and anti-mCherry (1:2,000 v/v, Abcam, ab125096) were used for western blot analysis.

Fluorescence and luminescence imaging. GFP images were obtained using a SteREO Discovery.V12 microscope (Zeiss). For the analysis of subcellular localization, imaging was performed using an LSM 7 DUO confocal laser microscopy microscope (Zeiss). Luminescence images were obtained using a NightShade LB985 in vivo plant imaging system (Berthold Technologies) by spraying with 1 mM luciferin solution containing 0.01% Triton X-100 using.

MG132 treatment. PORI plants were vertically grown on 1/2 MS media for 4–5 d and transferred to 1/2 MS media containing MG132 (100 μM) or DMSO. When the first and second true leaves were expanding 3 d after the transfer, the GFP signal was examined using fluorescence microscopy. To test the effect of MG132 on the DCP2 level, vertically grown nine-day-old pDCP2::DPC2-GFP transgenic seedlings were incubated in 1/2 MS liquid media in the absence and presence of MG132 (50 μM) for 36 h and used for western blot analysis.

Reporting Summary. Further information on research design is available in the Nature Research Reporting Summary linked to this article.

Data availability

sRNA sequencing data were deposited to Gene Expression Omnibus with accession no. GSE131009. All data needed to evaluate the conclusions in the paper are present in the paper and/or the supplementary materials. Additional data related to this paper may be requested from the authors. Source data for Figs. 1–4 and Extended Data Figs. 4, 6 and 8 are provided with the paper.

Received: 21 May 2019; Accepted: 9 October 2019;
Published online: 18 November 2019

References

1. Liu, L. & Chen, X. M. RNA quality control as a key to suppressing RNA silencing of endogenous genes in plants. *Mol. Plant* **9**, 826–836 (2016).
2. Schwab, R. & Voinnet, O. RNA silencing amplification in plants: size matters. *Proc. Natl Acad. Sci. USA* **107**, 14945–14946 (2010).
3. Schoenberg, D. R. & Maquat, L. E. Regulation of cytoplasmic mRNA decay. *Nat. Rev. Genet.* **13**, 246–259 (2012).
4. Tsuzuki, M., Motomura, K., Kumakura, N. & Takeda, A. Interconnections between mRNA degradation and RDR-dependent siRNA production in mRNA turnover in plants. *J. Plant Res.* **130**, 211–226 (2017).
5. Martinez de Alba, A. E. et al. In plants, decapping prevents RDR6-dependent production of small interfering RNAs from endogenous mRNAs. *Nucleic Acids Res.* **43**, 2902–2913 (2015).
6. Szadeczky-Kardoss, I. et al. The nonstop decay and the RNA silencing systems operate cooperatively in plants. *Nucleic Acids Res.* **46**, 4632–4648 (2018).
7. Zhang, X. et al. Suppression of endogenous gene silencing by bidirectional cytoplasmic RNA decay in *Arabidopsis*. *Science* **348**, 120–123 (2015).
8. Yu, A. et al. Second-site mutagenesis of a hypomorphic argonaute1 allele identifies SUPERKILLER3 as an endogenous suppressor of transgene posttranscriptional gene silencing. *Plant Physiol.* **169**, 1266–1274 (2015).
9. Gazzani, S., Lawrenson, T., Woodward, C., Headon, D. & Sablowski, R. A link between mRNA turnover and RNA interference in *Arabidopsis*. *Science* **306**, 1046–1048 (2004).
10. Zhao, L. & Kunst, L. SUPERKILLER complex components are required for the RNA exosome-mediated control of cuticular wax biosynthesis in *Arabidopsis* inflorescence stems. *Plant Physiol.* **171**, 960–973 (2016).
11. Collins, G. A. & Goldberg, A. L. The logic of the 26S proteasome. *Cell* **169**, 792–806 (2017).
12. Finley, D. Recognition and processing of ubiquitin–protein conjugates by the proteasome. *Annu. Rev. Biochem.* **78**, 477–513 (2009).
13. Groll, M. et al. Structure of 20S proteasome from yeast at 2.4 A resolution. *Nature* **386**, 463–471 (1997).
14. Finley, D., Chen, X. & Walters, K. J. Gates, channels, and switches: elements of the proteasome machine. *Trends Biochem. Sci.* **41**, 77–93 (2016).
15. Vierstra, R. D. The ubiquitin–26S proteasome system at the nexus of plant biology. *Nat. Rev. Mol. Cell Biol.* **10**, 385–397 (2009).
16. Lee, K. H. et al. The RPT2 subunit of the 26S proteasome directs complex assembly, histone dynamics, and gametophyte and sporophyte development in *Arabidopsis*. *Plant Cell* **23**, 4298–4317 (2011).
17. Smalle, J. et al. The pleiotropic role of the 26S proteasome subunit RPN10 in *Arabidopsis* growth and development supports a substrate-specific function in abscisic acid signaling. *Plant Cell* **15**, 965–980 (2003).
18. Smalle, J. et al. Cytokinin growth responses in *Arabidopsis* involve the 26S proteasome subunit RPN12. *Plant Cell* **14**, 17–32 (2002).
19. Stadler, R. & Sauer, N. The *Arabidopsis thaliana AtSUC2* gene is specifically expressed in companion cells. *Bot. Acta* **109**, 299–306 (1996).
20. Carbonell, A. et al. New generation of artificial microRNA and synthetic trans-acting small interfering RNA vectors for efficient gene silencing in *Arabidopsis*. *Plant Physiol.* **165**, 15–29 (2014).
21. Nadeau, J. A. & Sack, F. D. Control of stomatal distribution on the *Arabidopsis* leaf surface. *Science* **296**, 1697–1700 (2002).
22. Baumberger, N. & Baulcombe, D. C. *Arabidopsis* ARGONAUTE1 is an RNA slicer that selectively recruits rnicroRNAs and short interfering RNAs. *Proc. Natl Acad. Sci. USA* **102**, 11928–11933 (2005).
23. Ma, Z. & Zhang, X. Actions of plant Argonautes: predictable or unpredictable? *Curr. Opin. Plant Biol.* **45**, 59–67 (2018).
24. Mourrain, P. et al. *Arabidopsis SGS2* and *SGS3* genes are required for posttranscriptional gene silencing and natural virus resistance. *Cell* **101**, 533–542 (2000).
25. Dalmay, T., Hamilton, A., Rudd, S., Angell, S. & Baulcombe, D. C. An RNA-dependent RNA polymerase gene in *Arabidopsis* is required for posttranscriptional gene silencing mediated by a transgene but not by a virus. *Cell* **101**, 543–553 (2000).
26. Baulcombe, D. RNA silencing in plants. *Nature* **431**, 356–363 (2004).
27. Law, J. A. & Jacobsen, S. E. Establishing, maintaining and modifying DNA methylation patterns in plants and animals. *Nat. Rev. Genet.* **11**, 204–220 (2010).
28. Xie, M. & Yu, B. siRNA-directed DNA methylation in plants. *Curr. Genomics* **16**, 23–31 (2015).
29. Sonoda, Y. et al. Regulation of leaf organ size by the *Arabidopsis* RPT2a 19S proteasome subunit. *Plant J.* **60**, 68–78 (2009).
30. Sijacic, P., Wang, W. & Liu, Z. Recessive antimorphic alleles overcome functionally redundant loci to reveal *TSO1* function in *Arabidopsis* flowers and meristems. *PLoS Genet.* **7**, e1002352 (2011).
31. Parent, J. S. et al. Post-transcriptional gene silencing triggered by sense transgenes involves uncapped antisense RNA and differs from silencing intentionally triggered by antisense transgenes. *Nucleic Acids Res.* **43**, 8464–8475 (2015).
32. Smith, L. M. et al. An SNF2 protein associated with nuclear RNA silencing and the spread of a silencing signal between cells in *Arabidopsis*. *Plant Cell* **19**, 1507–1521 (2007).
33. Martinez de Alba, A. E., Elvira-Matelot, E. & Vaucheret, H. Gene silencing in plants: a diversity of pathways. *Biochim. Biophys. Acta* **1829**, 1300–1308 (2013).
34. Miki, D. et al. Efficient generation of diRNAs requires components in the posttranscriptional gene silencing pathway. *Sci. Rep.* **7**, 301 (2017).
35. Motomura, K. et al. The role of decapping proteins in the miRNA accumulation in *Arabidopsis thaliana*. *RNA Biol.* **9**, 644–652 (2012).
36. Hooker, T. S., Lam, P., Zheng, H. & Kunst, L. A core subunit of the RNA-processing/degrading exosome specifically influences cuticular wax biosynthesis in *Arabidopsis*. *Plant Cell* **19**, 904–913 (2007).
37. Moreno, A. B. et al. Cytoplasmic and nuclear quality control and turnover of single-stranded RNA modulate post-transcriptional gene silencing in plants. *Nucleic Acids Res.* **41**, 4699–4708 (2013).
38. Shin, J. H. et al. The role of the *Arabidopsis* exosome in siRNA-independent silencing of heterochromatic loci. *PLoS Genet.* **9**, e1003411 (2013).
39. Lam, P. et al. The exosome and trans-acting small interfering RNAs regulate cuticular wax biosynthesis during *Arabidopsis* inflorescence stem development. *Plant Physiol.* **167**, 323–336 (2015).
40. Branscheid, A. et al. SKI2 mediates degradation of RISC 5′-cleavage fragments and prevents secondary siRNA production from miRNA targets in *Arabidopsis*. *Nucleic Acids Res.* **43**, 10975–10988 (2015).
41. Erickson, S. L. et al. Competition between decapping complex formation and ubiquitin-mediated proteasomal degradation controls human Dcp2 decapping activity. *Mol. Cell Biol.* **35**, 2144–2153 (2015).

42. Kelly, S. P. & Bedwell, D. M. Both the autophagy and proteasomal pathways facilitate the Ubp3p-dependent depletion of a subset of translation and RNA turnover factors during nitrogen starvation in *Saccharomyces cerevisiae*. *RNA* **21**, 898–910 (2015).
43. Stribinskis, V. & Ramos, K. S. Rpm2p, a protein subunit of mitochondrial RNase P, physically and genetically interacts with cytoplasmic processing bodies. *Nucleic Acids Res.* **35**, 1301–1311 (2007).
44. Brengues, M., Teixeira, D. & Parker, R. Movement of eukaryotic mRNAs between polysomes and cytoplasmic processing bodies. *Science* **310**, 486–489 (2005).
45. Graham, A. C., Kiss, D. L. & Andrulis, E. D. Differential distribution of exosome subunits at the nuclear lamina and in cytoplasmic foci. *Mol. Biol. Cell* **17**, 1399–1409 (2006).
46. Goldberg, A. L. Protein degradation and protection against misfolded or damaged proteins. *Nature* **426**, 895–899 (2003).
47. Erales, J., Hoyt, M. A., Troll, F. & Coffino, P. Functional asymmetries of proteasome translocase pore. *J. Biol. Chem.* **287**, 18535–18543 (2012).
48. Kilian, J. et al. The AtGenExpress global stress expression data set: protocols, evaluation and model data analysis of UV-B light, drought and cold stress responses. *Plant J.* **50**, 347–363 (2007).
49. Sakamoto, T. et al. *Arabidopsis thaliana* 26S proteasome subunits RPT2a and RPT5a are crucial for zinc deficiency-tolerance. *Biosci. Biotechnol. Biochem.* **75**, 561–567 (2011).
50. Sako, K. et al. Proteomic analysis of the 26S proteasome reveals its direct interaction with transit peptides of plastid protein precursors for their degradation. *J. Proteome Res.* **13**, 3223–3230 (2014).
51. Lange, H. et al. The RNA helicases AtMTR4 and HEN2 target specific subsets of nuclear transcripts for degradation by the nuclear exosome in *Arabidopsis thaliana*. *PLoS Genet.* **10**, e1004564 (2014).
52. Li, H. & Durbin, R. Fast and accurate short read alignment with Burrows–Wheeler transform. *Bioinformatics* **25**, 1754–1760 (2009).
53. McKenna, A. et al. The Genome Analysis Toolkit: a MapReduce framework for analyzing next-generation DNA sequencing data. *Genome Res.* **20**, 1297–1303 (2010).
54. Martin, M. CUTADAPT removes adapter sequences from high-throughput sequencing reads. *EMBnet J.* **17**, 10–12 (2011).
55. Johnson, N. R., Yeoh, J. M., Coruh, C. & Axtell, M. J. Improved placement of multi-mapping small RNAs. *G3* **6**, 2103–2111 (2016).
56. Love, M. I., Huber, W. & Anders, S. Moderated estimation of fold change and dispersion for RNA-seq data with DESeq2. *Genome Biol.* **15**, 550 (2014).
57. Robinson, M. D., McCarthy, D. J. & Smyth, G. K. edgeR: a Bioconductor package for differential expression analysis of digital gene expression data. *Bioinformatics* **26**, 139–140 (2010).
58. Benjamini, Y. & Hochberg, Y. Controlling the false discovery rate—a practical and powerful approach to multiple testing. *J. R. Stat. Soc. B* **57**, 289–300 (1995).
59. Langmead, B., Trapnell, C., Pop, M. & Salzberg, S. L. Ultrafast and memory-efficient alignment of short DNA sequences to the human genome. *Genome Biol.* **10**, R25 (2009).
60. Wu, H. W., Lin, S. S., Chen, K. C., Yeh, S. D. & Chua, N. H. Discriminating mutations of HC-Pro of zucchini yellow mosaic virus with differential effects on small RNA pathways involved in viral pathogenicity and symptom development. *Mol. Plant Microbe Interact.* **23**, 17–28 (2010).

Acknowledgements

We thank Y. Watanabe for the pDCP2-DCP2-GFP transgenic line, H. Lange for the RRP41-GFP and RRP41-MYC transgenic plants, H. Vaucheret for the L1 line, S. Park for the JAP3 transgenic plants, C. You and J. H. Park for the technical advice. This work was supported by IBS-R013-G2 from the Institute for Basic Science and in part by a grant from National Research Foundation (2019R1A2C3007376) and start-up funds from DGIST to J.M.K., and in part by (IBS-R013-D1) from the Institute for Basic Science.

Author contributions

Y.J.K. and J.M.K. conceived the study and designed the experiments. M.-H.K., J.J., S.L. and J.M.P. performed the experiments. J.H.L. and L.G. analysed WGS and sRNA sequencing data. B.-H.L., Y.J.K. and J.M.K. wrote the manuscript.

Competing interests

The authors declare no competing interests.

Additional information

Extended data is available for this paper at https://doi.org/10.1038/s41477-019-0546-1.

Supplementary information is available for this paper at https://doi.org/10.1038/s41477-019-0546-1.

Correspondence and requests for materials should be addressed to Y.J.K. or J.M.K.

Peer review information: *Nature Plants* thanks Xiuren Zhang and the other, anonymous, reviewer(s) for their contribution to the peer review of this work.

Reprints and permissions information is available at www.nature.com/reprints.

Publisher's note Springer Nature remains neutral with regard to jurisdictional claims in published maps and institutional affiliations.

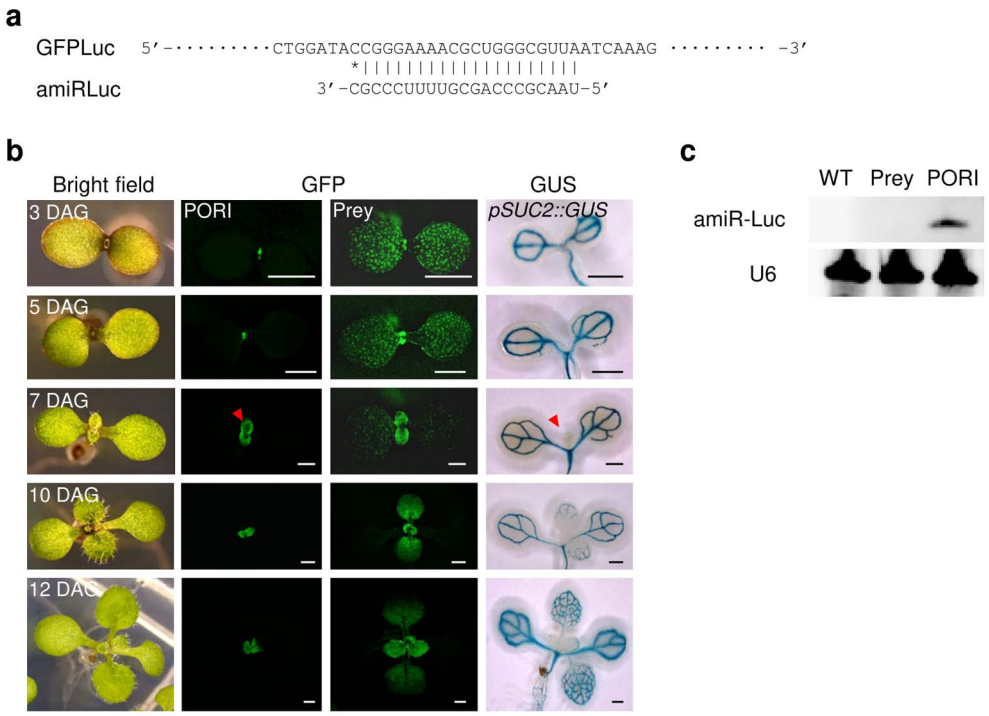

Extended Data Fig. 1 | Phenotypes of PORI plants. (**a**) amiR-Luc sequence targeting GFPLuc. (**b**) Spatiotemporal GFP expression patterns in the prey, the Orion and the PORI plants. The cell type-specific expression of the TMM and SUC2 promoters were examined in transgenic plants harbouring the *pTMM::GFP* or *pSUC2::GUS* constructs. The arrowheads indicate a developing leaf where the GFP or the GUS expression is initiated and then disappeared or maintained, respectively. Scale bar, 1 mm. At least ten independent plants showed similar results. (**c**) Northern blot analysis of the accumulation of amiR-Luc in WT, prey, and PORI plants. U6 RNA was used as a loading control. The experiment was independently repeated four times with similar results.

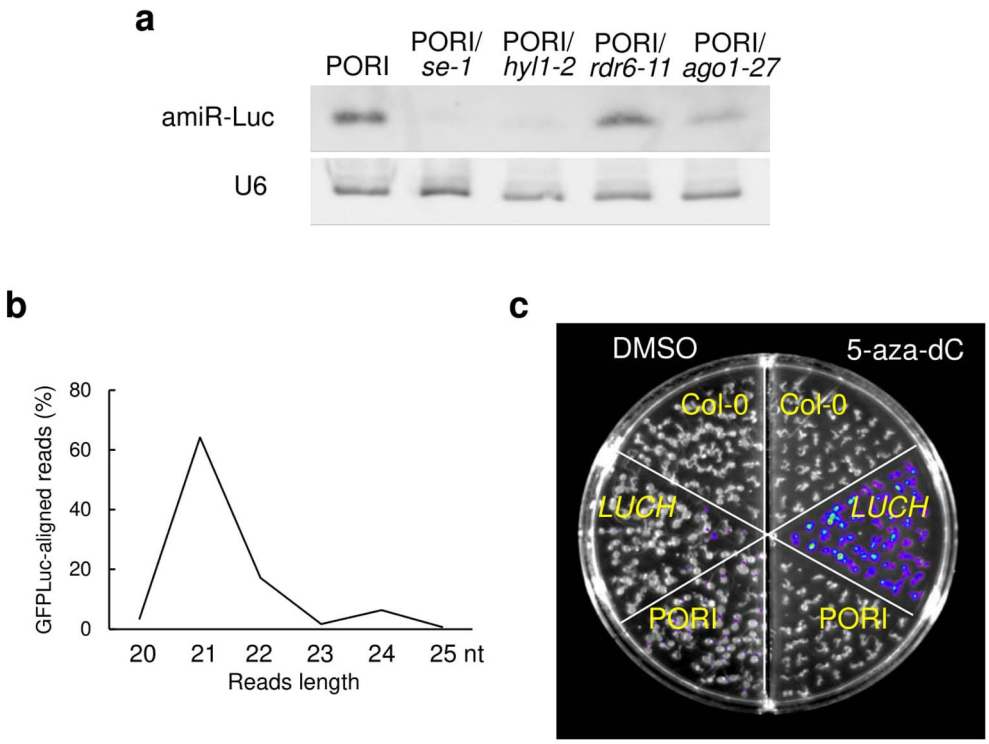

Extended Data Fig. 2 | Production of amiR-Luc in PORI plants is not regulated by the transcriptional gene silencing machinery. (**a**) Northern blot analysis of amiR-Luc in the PORI and PORI/*se-1*, PORI/*hyl-1*, PORI/*rdr6-11*, and PORI/*ago1-27*. U6 RNA was used as a loading control. The experiment was independently repeated three times with similar results. (**b**) The size distribution of GFPLuc-siRNAs in the PORI plants. Data represent the mean of two independent replicates. (**c**) Luciferase activities in WT, LUCH, and PORI seedlings at 5 DAG in the absence or presence of 5-aza-dC. LUCH seedlings were used as a positive control. The experiment was independently repeated three times with similar results.

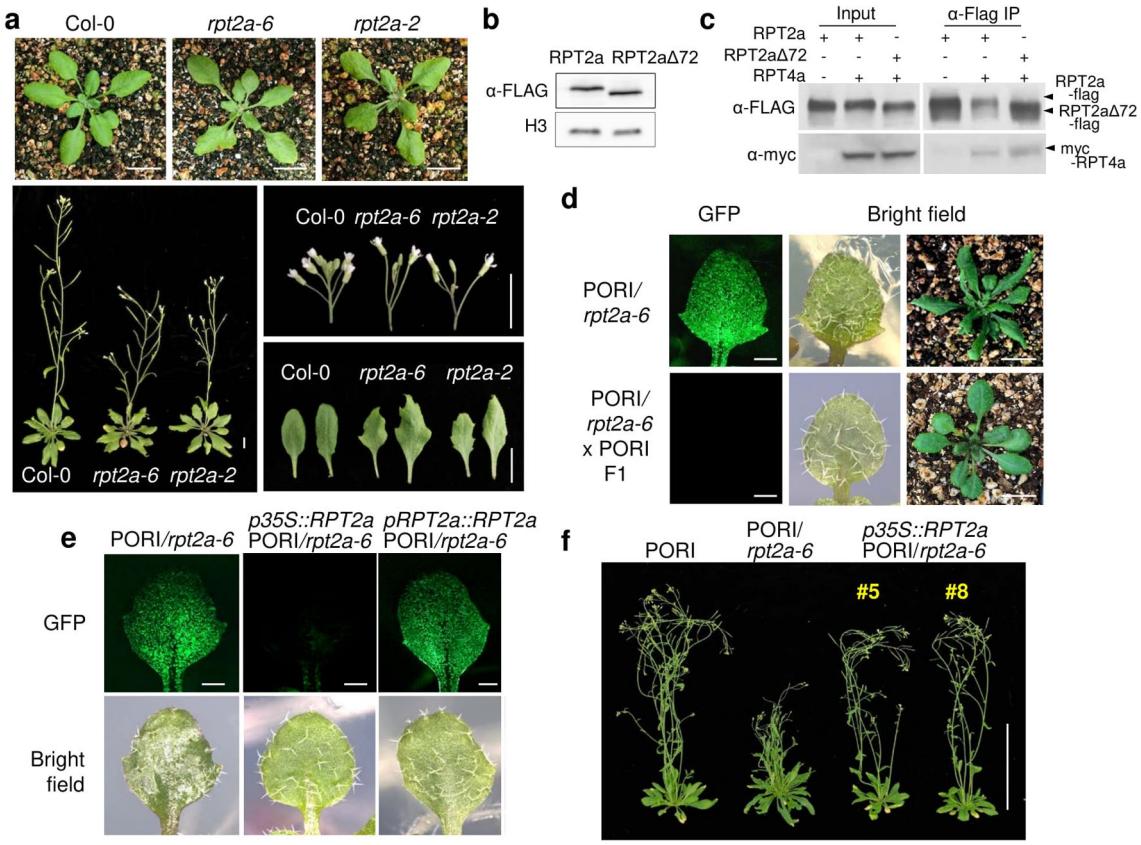

Extended Data Fig. 3 | RPT2a plays a role in the suppression of GFP in PORI plants. (**a**) Morphological phenotypes of rosette leaves, inflorescence, and size of Col, rpt2a-2, and rpt2a-6 plants. Scale bar, 1 cm. The segregation analysis of progenies from the genetic crosses is shown in Supplementary Table 1. (**b**) The detection of transiently expressed RPT2a and RPT2aΔ72bp in tobacco by western blot analysis. The experiment was repeated two times with similar results. (**c**) Co-immunoprecipitation analysis shows the interaction between RPT2a/RPT2aΔ72bp and RPT4a. RPT2a-flag, RPT2aΔ72bp-flag, and myc-RPT4a were expressed in tobacco plants. The experiment was repeated two times with similar results. (**d**) Allelic test among PORI, PORI/*rpt2a-2* and PORI/*rpt2a-6* plants. GFP fluorescence and morphological phenotypes of F1 plants. Scale bar, 500 μm (GFP), 1 cm (plants). The segregation analysis of progenies from the genetic crosses is shown in Supplementary Table 1. (**e**, **f**) Complementation test of PORI/*rpt2a-6* by expressing *p35S::RPT2a* or *pRPT2a::RPT2a*. GFP fluorescence (**e**) and morphological phenotypes (**f**) of transgenic plants carrying *p35S::RPT2a* or *pRPT2a::RPT2a* in PORI/*rpt2a-6*. Scale bar, 500 μm (**e**), 10 cm (**f**). At least five independent transgenic plants showed similar results.

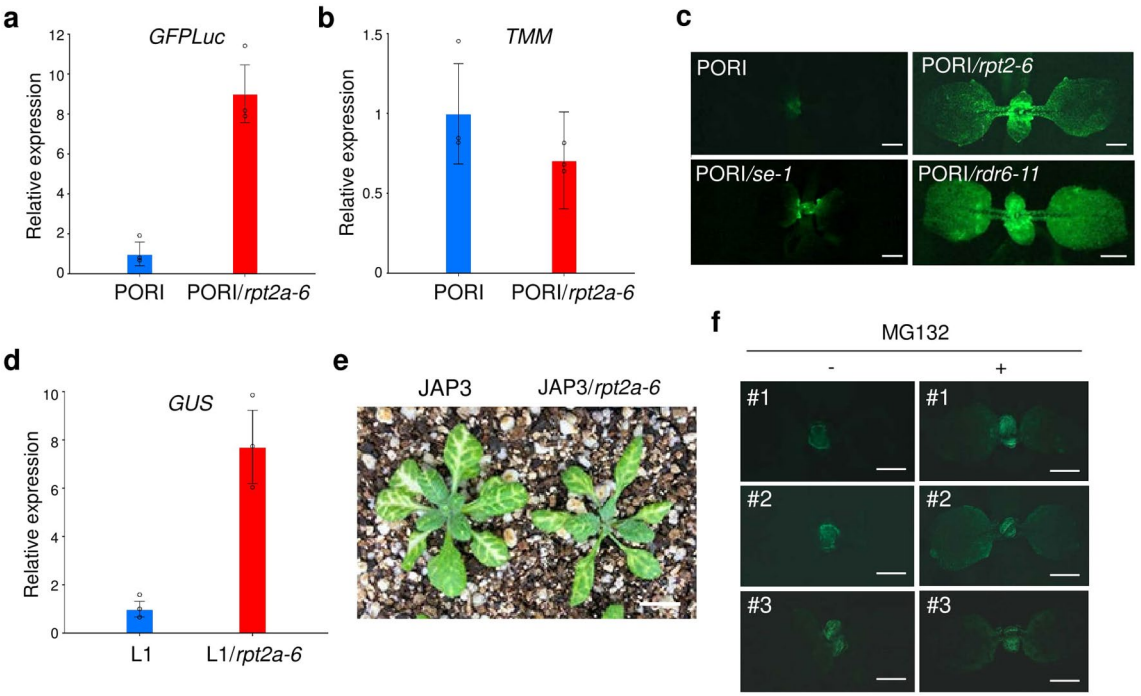

Extended Data Fig. 4 | RPT2a promotes S-PTGS but not IR-PTGS. (**a**, **b**) qRT-PCR analyses of GFPLuc (**a**) and TMM transcripts (**b**) in PORI and PORI/rpt2-6 plants. (c) GFP expression patterns of PORI, PORI/*rpt2a-6*, PORI/*se-1*, and PORI/*rdr6-11* plants. Scale bar, 600 μm. The segregation analysis of progenies from the genetic crosses is shown in Supplementary Table 1. (**d**) qRT-PCR analysis GUS transcripts in L1 and L1/*rpt2a-6* plants. (**a**, **b**, **d**) The expression levels were normalized to UBQ5 (At3g62250). Error bars represent mean ± s.d. from three independent biological replicates. (**e**) Photobleaching phenotypes in the IR-PTGS reporter JAP3 plants and JAP3/*rpt2a-6*. Scale bar, 1 cm. The segregation analysis of progenies from the genetic crosses is shown in Supplementary Table 1. (**f**) GFP fluorescence in the PORI plants treated with and without MG132. Scale bar, 1 mm. The experiment was independently repeated at least three times with similar results.

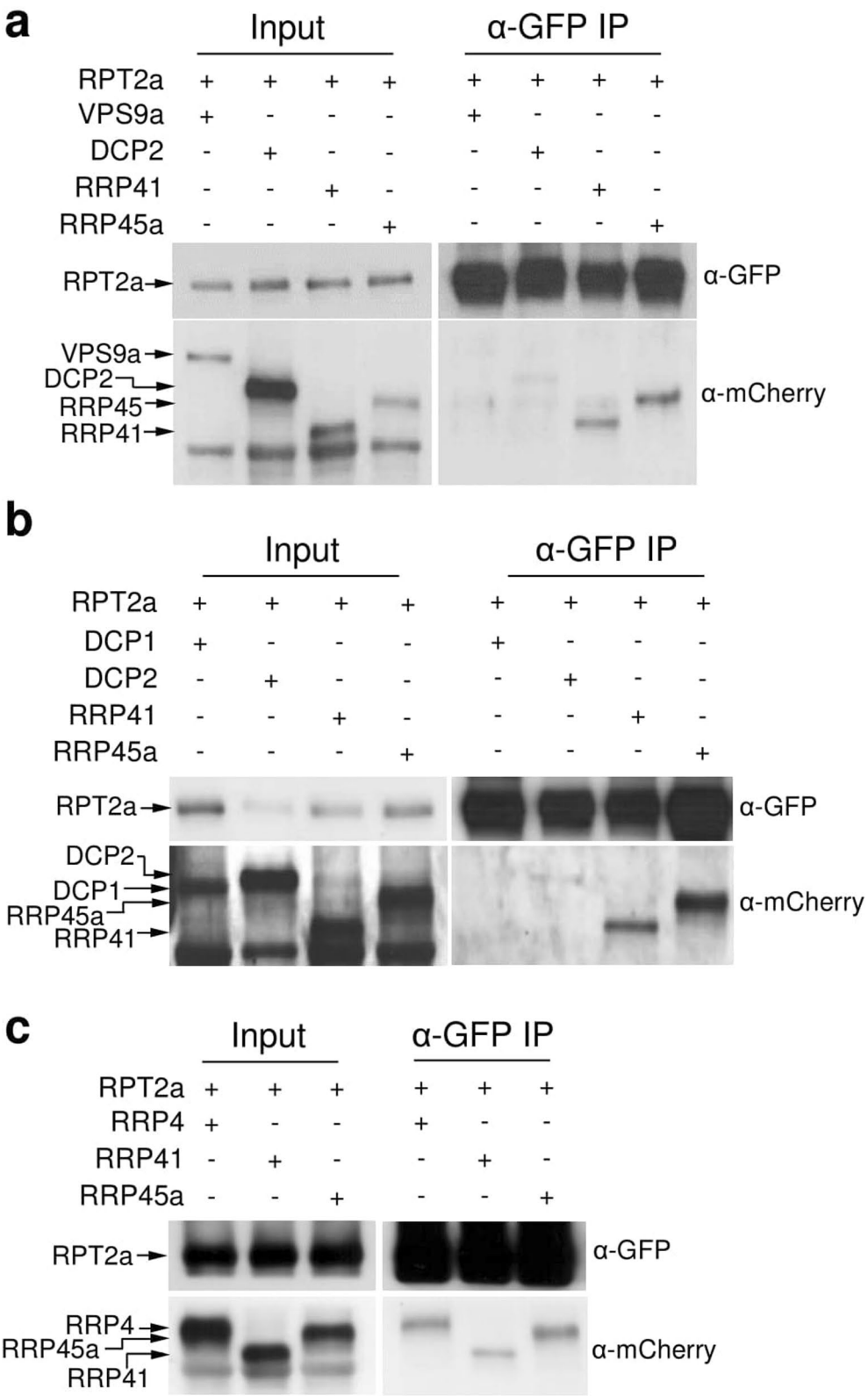

Extended Data Fig. 5 | In vivo interaction between RPT2a and a subset of the RQC components, DCP2, RRP41 and RRP45a. VPS9a (AT3G19770) (**a**), DCP1 (**b**) and RRP4 (**c**) were used as negative controls. RPT2a-GFP, RRP41-mCherry, RRP45a-mCherry, DCP2-mCherry, DCP1-mCherry, RRP4-mCherry, and VPS9a-mCherry were expressed in tobacco plants expressing SGS3-CFP. The experiment was independently repeated at least two times with similar results.

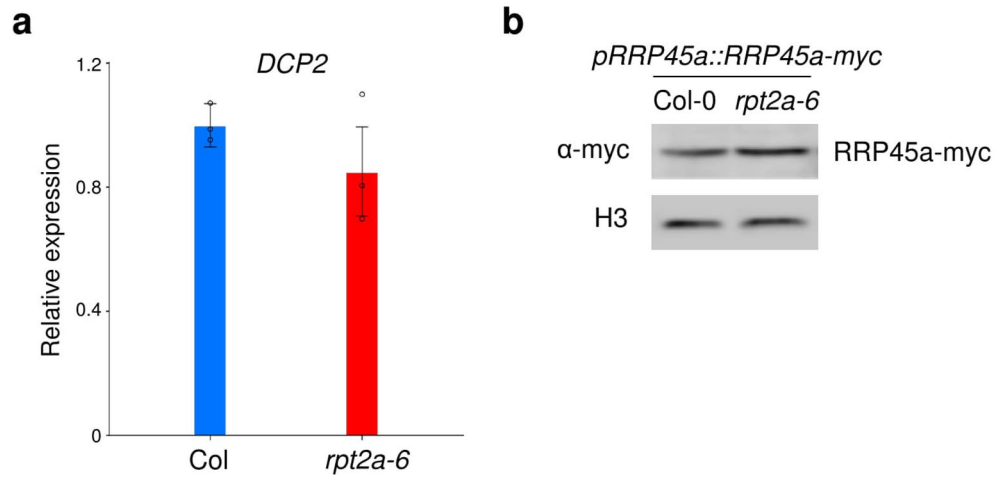

Extended Data Fig. 6 | Transcript and protein levels of DCP2 and RRP45a in *rpt2a-6*. (**a**) qRT-PCR analysis reveals the expression level of DCP2 in WT and *rpt2a-6* plants normalized to UBQ5. Error bars represent mean ± s.d. calculated from three biological replicates. (**b**) Western blot analysis of RRP45a proteins in WT and *rpt2a-6*. The experiment was independently repeated three times with similar results.

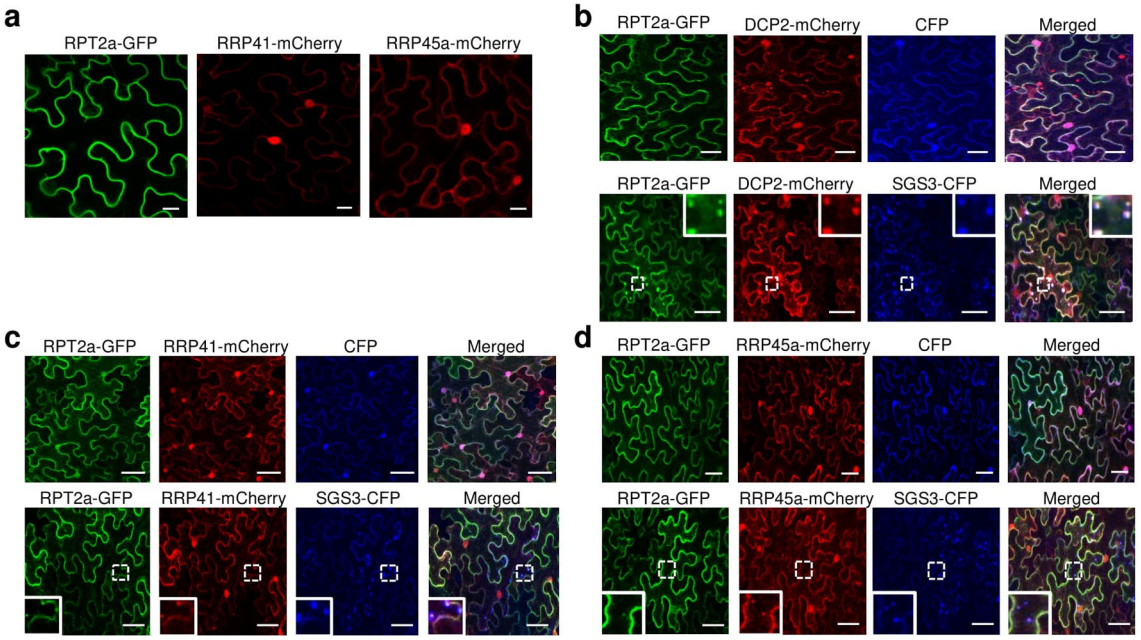

Extended Data Fig. 7 | RPT2a is translocated to cytoplasmic speckles in presence of SGS3. (**a**) Subcellular localization of RPT2a, RRP41, and RRP45a. (**b**–**d**) Subcellular localization of RPT2a with DCP2 (**b**), RRP41 (**c**), and RRP45a (**d**) in the absence or presence of SGS3. The inset is an enlarged view of the region in the white box, in which a subset of co-localized granules of RPT2a and SGS3 are present in combination with DCP2, RRP41, or RRP45a. The proteins were transiently expressed in tobacco leaves. Scale bar, 20 μm (**a**), 50 μm (**b**–**d**). The experiment was independently repeated at least five times with similar results.

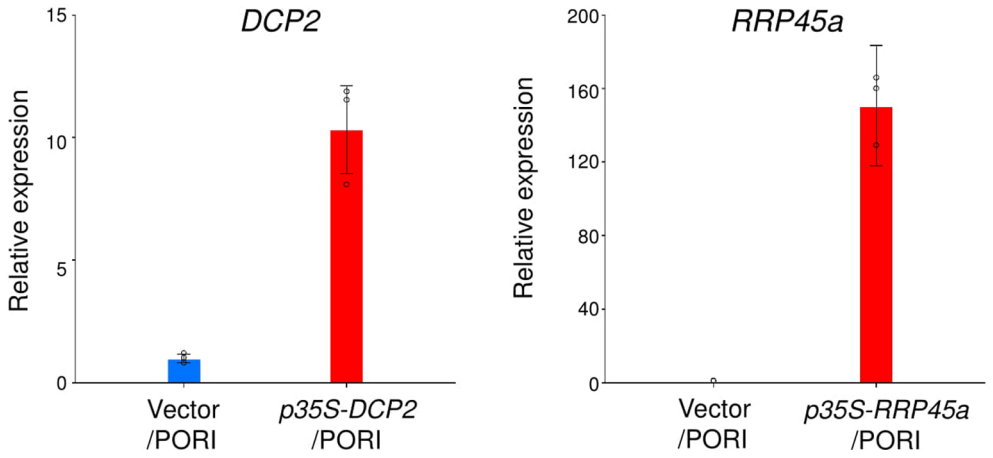

Extended Data Fig. 8 | Transcript levels of *DCP2* and *RRP45a* in 35s-DCP2 and 35s-RRP45a transgenic plants. qRT-PCR reveals the expression levels of *DCP2* and *RRP45a* in p35s-DCP2 and p35s-RRP45a transgenic plants. The relative expression values were obtained by normalization to *UBQ5*. Error bars represent mean ± s.d. calculated from three independent biological replicates.

nature research

Corresponding author(s): Yun Ju Kim, June M. Kwak

Last updated by author(s): 10-07-2019

Reporting Summary

Nature Research wishes to improve the reproducibility of the work that we publish. This form provides structure for consistency and transparency in reporting. For further information on Nature Research policies, see Authors & Referees and the Editorial Policy Checklist.

Statistics

For all statistical analyses, confirm that the following items are present in the figure legend, table legend, main text, or Methods section.

n/a	Confirmed	
☐	☒	The exact sample size (*n*) for each experimental group/condition, given as a discrete number and unit of measurement
☐	☒	A statement on whether measurements were taken from distinct samples or whether the same sample was measured repeatedly
☐	☒	The statistical test(s) used AND whether they are one- or two-sided *Only common tests should be described solely by name; describe more complex techniques in the Methods section.*
☐	☒	A description of all covariates tested
☐	☒	A description of any assumptions or corrections, such as tests of normality and adjustment for multiple comparisons
☐	☒	A full description of the statistical parameters including central tendency (e.g. means) or other basic estimates (e.g. regression coefficient) AND variation (e.g. standard deviation) or associated estimates of uncertainty (e.g. confidence intervals)
☐	☒	For null hypothesis testing, the test statistic (e.g. *F*, *t*, *r*) with confidence intervals, effect sizes, degrees of freedom and *P* value noted *Give P values as exact values whenever suitable.*
☒	☐	For Bayesian analysis, information on the choice of priors and Markov chain Monte Carlo settings
☒	☐	For hierarchical and complex designs, identification of the appropriate level for tests and full reporting of outcomes
☒	☐	Estimates of effect sizes (e.g. Cohen's *d*, Pearson's *r*), indicating how they were calculated

Our web collection on statistics for biologists contains articles on many of the points above.

Software and code

Policy information about availability of computer code

Data collection	For the DNASeq and sRNASeq : -Illumina Truseq Nano DNA Libary prep protocol. (Hiseq 2500 system. 101 cycles paired end read) -Illumina NEBNext Multiplex Small RNA library prep protocol. (Hiseq 2500 system. 50bp single end read)
Data analysis	For the DNASeq analysis : - sickle v1.31 - BWA v0.7.12 - Picard MarkDuplicates v1.119 - Genome Analysis Toolkit 3.5 (GATK) - FastQC v0.11.2 For the sRNASeq analysis: - FastQC v0.11.2 - pRNASeqTools pipeline : cutadapter v1.9.1 : Bowtie v1.1.2 : ShorStack v3.4 : R (DESeq2)v3.4.0 - EdgeR v3.24.0. For the gene expression analysis - GraphPad Prism 7 - R (ggplot,gplots) v3.4.2

For manuscripts utilizing custom algorithms or software that are central to the research but not yet described in published literature, software must be made available to editors/reviewers. We strongly encourage code deposition in a community repository (e.g. GitHub). See the Nature Research guidelines for submitting code & software for further information.

Data

Policy information about availability of data

All manuscripts must include a data availability statement. This statement should provide the following information, where applicable:

- Accession codes, unique identifiers, or web links for publicly available datasets
- A list of figures that have associated raw data
- A description of any restrictions on data availability

sRNA-seq data were deposited to the GenBank with accession no. GSE131009.
There is no restriction on data availability.
All relevant data are available from the corresponding authors upon request.

Field-specific reporting

Please select the one below that is the best fit for your research. If you are not sure, read the appropriate sections before making your selection.

☒ Life sciences ☐ Behavioural & social sciences ☐ Ecological, evolutionary & environmental sciences

For a reference copy of the document with all sections, see nature.com/documents/nr-reporting-summary-flat.pdf

Life sciences study design

All studies must disclose on these points even when the disclosure is negative.

Sample size	For most analyses of gene/protein expression and florescence imaging, 3 days, 5 days, 7-8 days or 10 days old seedlings (aerial part only) were used because the seedlings on those days were good enough to show differences in phenotype between the control and mutant plants. GUS activity and GUS-siRNA expression were analyzed using 14 days old seedlings. Other plant materials that were used to show morphological phenotypes and complementation were at least 21-day old. To minimize individual variation, 10-15 and 6-7 seedlings were pooled and used for RNA and protein extraction, respectively.
Data exclusions	No data were excluded from the analysis.
Replication	All data were repeated at least three time (except Fig. 2e, Fig. S3b,c, Fig. S5c and sRNA-seq, which were repeated two times) to confirm reproducibility except the sRNA-seq analysis and showed similar results. For the yeast two hybrid assays, more than three independent colonies were tested for the interaction.
Randomization	Arabidopsis plants grown under the same conditions were randomly selected based on the size and healthiness, harvested and processed for RNA extraction (10-15 seedlings) and protein extraction (6-7 seedlings).
Blinding	For the genetic analysis of the mutants, phenotyping and genotyping were separately processed. The phenotype information was first collected and matched with the genotype to confirm the phenotype-genotype correlation.

Reporting for specific materials, systems and methods

We require information from authors about some types of materials, experimental systems and methods used in many studies. Here, indicate whether each material, system or method listed is relevant to your study. If you are not sure if a list item applies to your research, read the appropriate section before selecting a response.

Materials & experimental systems

n/a	Involved in the study
☐	☒ Antibodies
☒	☐ Eukaryotic cell lines
☒	☐ Palaeontology
☒	☐ Animals and other organisms
☒	☐ Human research participants
☒	☐ Clinical data

Methods

n/a	Involved in the study
☒	☐ ChIP-seq
☒	☐ Flow cytometry
☒	☐ MRI-based neuroimaging

Antibodies

Antibodies used	anti-c-Myc-HRP antibody,1:4,000 v/v, Abcam, Catalog No. ab19312, Lot No. GR3193537-17 anti-eGFP antibody,1:1,000 v/v, Pierce, Catalog No. CAB4211, Lot No. TG267933 anti-FLAG M2-Peroxidase (HRP) antibody, 1:3000 v/v, Sigma, Catalog No. A8592, Lot No. SLBV3799 anti-Histone H3 antibody, 1:10,000 v/v, Abcam, Catalog No. ab1791, Lot No. GR203824-1 anti-mCherry antibody, 1:2000 v/v, Abcam, Catalog No. ab125096, Lot No. GR3234427-1, Clone No. 1C51

Validation

anti-c-Myc-HRP (https://www.abcam.com/c-myc-antibody-hrp-ab19312.html),
anti-eGFP (https://www.thermofisher.com/antibody/product/eGFP-Antibody-Polyclonal/CAB4211),
anti-FLAG M2-Peroxidase (HRP) (https://www.sigmaaldrich.com/catalog/product/sigma/a8592?lang=ko&region=KR),
anti-mCherry (https://www.abcam.com/mcherry-antibody-1c51-ab125096.html) are commercially available and the information for validation can be found at the link.
A single band at the predicted size was detected from the plants expressing each epitope-fused transgene, which was absent in the control plants in our experiments.
Anti-Histone H3 antibody has been used in many studies including (Kim et al.,PNAS, 2016, 113 (51), 14858-14863 and https://www.abcam.com/histone-h3-antibody-nuclear-loading-control-and-chip-grade-ab1791.html), and it produced a clear band in our western blot analysis.